# Development of a High-Sensitivity Triple-Band Nano-Biosensor Utilizing Petahertz Metamaterials for Optimal Absorption in Early-Stage Leukemia Detection

Musa N. Hamza, Mohammad Tariqul Islam, *Senior Member, IEEE*, Sunil Lavadiya, *Member, IEEE*, Iftikhar ud Din, Bruno Cavalcante de Souza Sanches, *Member, IEEE*, Slawomir Koziel, *Fellow, IEEE*, Syeda Iffat Naqvi, *Senior Member, IEEE*, Ali Farmani, *Member, IEEE*, and Md. Shabiul Islam, *Senior Member, IEEE*

***Abstract*—This research focuses on designing a novel miniaturized biosensor for early-stage detection of leukemia. The proposed sensor operates in the low petahertz (PHz) range. The primary prerequisites for the development process include multiband operation, compact physical size, near-perfect absorption at resonant frequencies, and insensitivity to the angle of incidence. These features are crucial for ensuring high-performance operation in microwave imaging (MWI) and have been achieved through meticulous design of the absorber's geometry and dimensions. The sensor incorporates a dipole and two rings made of gold or silver, implanted on a silicon dioxide ($SiO_2$) dielectric substrate with a fully metallic backplane. The evolution of the biosensor's topology is detailed, along with comprehensive simulation studies conducted using a commercial full-wave electromagnetic (EM) solver. The operating principles are explained through parametric studies, analysis of absorption and refraction characteristics, discussions of electric and magnetic fields, and surface current density distributions. The device's suitability for blood cancer diagnostics is demonstrated through full-wave analysis of the MWI system, highlighting the sensor's ability to discriminate between healthy and cancerous samples through noticeable frequency shifts in absorption responses. Extensive comparisons with the state-of-the-art biosensors reported in recent literature show that the proposed device significantly improves spectral properties and achieves remarkable spatial resolution due to its PHz range operation when compared to the benchmark.**

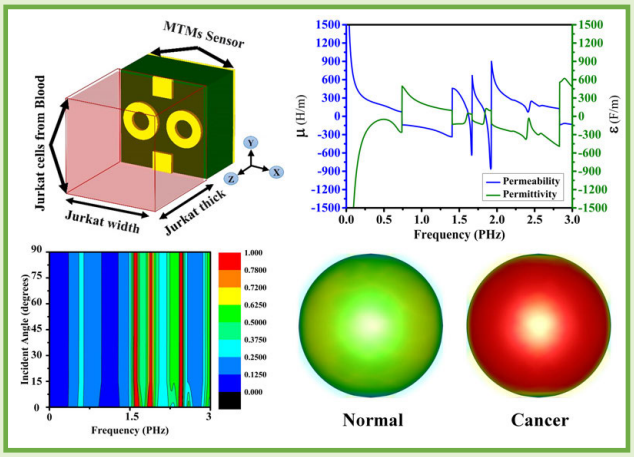


***Index Terms*— Blood cancer, metamaterials (MTMs), microwave imaging (MWI) technique, nano-biosensors, perfect absorber.**

## I. Introduction

CANCER is one of the most formidable diseases encountered by humans. There is an estimation that by 2030, nearly 17 million people will die from cancer-related health issues, and 26 million new cases of cancer will be diagnosed [1], [2]. Blood malignancy, known as leukemia, is considered to be a particularly aggressive disease. Leukemia, a type of blood cancer, originates from bone marrow cells and results in the development and proliferation of abnormal blood cells. This condition disrupts the normal production of blood cells in the bone marrow [3]. The prevalence of blood cancers is increasing annually due to genetic and environmental factors. According to the American Cancer Society, leukemia is the second major cause of death in children, adolescents, and young people under the age of 20, making it the most common cancer type affecting children [4], [5]. Every three minutes, one person is diagnosed with leukemia, a disease that can be found in two forms: acute, where leukemia cells

Received 5 February 2025; accepted 16 February 2025. Date of publication 4 March 2025; date of current version 16 April 2025. This work was supported in part by the University of Doha for Science and Technology under Grant KK-2024-005, in part by the Icelandic Research Fund under Grant 239858, and in part by the National Science Centre of Poland under Grant 2020/37/B/ST7/01448. The associate editor coordinating the review of this article and approving it for publication was Dr. Chirasree Roychaudhuri. *(Corresponding authors: Musa N. Hamza; Mohammad Tariqul Islam; Md. Shabiul Islam.)*

Please see the Acknowledgment section of this article for the author affiliations.

Digital Object Identifier 10.1109/JSEN.2025.3544761

multiply quickly, and chronic, where the cancer progresses gradually with initially mild symptoms. Leukemia can further be classified based on the type of cell it originates from such as myeloid cells (granulocytes or monocytes) or lymphocyte cells (B-cells, T-cells, or natural killer cells). The four main types of leukemia are chronic myelogenous leukemia (CML), chronic lymphocytic leukemia (CLL), acute myelogenous leukemia (AML), and acute lymphocytic leukemia (ALL) [6], [7]. Myeloid cell-origin leukemias include AML and CML, whereas lymphocyte-origin leukemias include ALL and CLL. ALL and AML being most common in children and adults, respectively, have incidence and mortality rates ranking 15th and 10th for all malignant cases [8]. ALL is a lethal illness causing rapid and excessive proliferation and accumulation of immature B and T lymphocytes in the bone marrow, blood, and extramedullary locations, preventing the production of normal white blood cells. These immature leukemic cells, known as lymphoblasts, are incapable of fighting infections as effectively as normal white blood cells. The prognosis for elderly patients with ALL remains poor despite advancements in dose-intensification methods that have shown encouraging results in pediatric cases. Only 30%–40% of adult patients with ALL achieve long-term remission [9]. Early detection of ALL is critical for successful treatment outcomes, particularly in children. However, the diagnostic process is complicated by the similarities between normal and malignant lymphoid cells, which makes distinguishing them challenging. Accurate diagnosis necessitates the manual examination of bone marrow samples, a process that is not only time-consuming but also highly dependent on the pathologist's expertise. Despite their crucial role, pathologists are still prone to human error. Consequently, achieving an early and accurate diagnosis is vital for improving recovery rates, and also to minimize the worldwide impact of leukemia on public health [10].

Refractive index (RI) sensors have been extensively explored for biomedical applications due to their crucial role in real-time biosensing. The measurement of RI provides essential parameters for material characterization, including mass density, concentration, and pressure. Prior research [11] introduced a multilayered metamaterial (MTM) absorber that achieves perfect absorption by leveraging the epsilon-near-zero (ENZ) mode. In the present study, the sensitivity of this structure to variations in the surrounding RI is utilized for RI sensing. This absorber exhibits significant potential in optical communication systems, where it can serve as a component for filters, detectors, and sensing devices.

Beyond optical communication, RI sensors have gained prominence in medical diagnostics, particularly in monitoring cancer progression through the detection of specific biomarkers. Their capability to track alterations in biological environments makes them valuable tools for the early detection of malignancies. A study in [12] proposed an optically tunable light absorber designed as an RI MTM biosensor for applications such as chemical sensing, monitoring glucose concentrations in aqueous solutions, and detecting viral particles. The operational principle of this multiband super-absorber nanostructure is based on resonance frequency shifts that occur in response to changes in the RI of the surrounding medium, enabling precise and efficient detection in diverse biomedical applications.

Because of the near-perfect absorption, perfect absorbers have been used for enhanced sensitivity in RI sensing for label-free detection of trivial changes and can operate over a broad range of refractive indices. These absorbers have diverse applications as they are adaptable at various frequencies [13]. Absorber models with complex structures based on quantum mechanics are currently being investigated by researchers for petahertz (PHz) applications. Perfect absorbers are expected to have higher efficiency and broadband operation, with angular and polarization insensitivity, so innovative design methods and components are currently being explored [14]. There have been many suggestions aimed at envisioning of biosensors from gigahertz to terahertz (THz) and well into PHz regions [13], [15], [16], [17], [18].

MTMs have gained significant attention as a fundamental component for achieving resonant frequencies within specific spectral ranges. Their ability to manipulate electromagnetic (EM) and optical properties has led to a broad spectrum of applications, including biosensing, imaging, antenna engineering, and optoelectronic systems [19], [20], [21], [22], [23], [24], [25], [26], [27], [28], [29], [30], [31], [32], [33], [34], [35], [36], [37], [38], [39], [40], [41], [42], [43], [44], [45], [46], [47], [48], [49], [50], [51], [52], [53]. For instance, the study presented in [38] introduced a compact, multiband MTM-based sensor designed for the early detection of cancer, operating within the THz frequency range. The primary focus of that work was to optimize the geometrical parameters to attain near-perfect absorption of EM waves across the designated operating bandwidth.

Furthermore, THz plasmonic sensors have been recognized as a promising advancement in biomedical applications due to their ability to provide real-time, label-free, and highly sensitive detection. The research outlined in [54] proposed a THz sensor with direct phase readout functionality, achieved by integrating steerable plasmonic resonance with attenuated total reflection. Beyond the THz spectrum, the sub-THz frequency range (below 1 THz) has also demonstrated potential for communication and sensing applications. The study presented in [55] introduced a metasurface-based absorber with an N-beam absorption peak configuration in the sub-THz range. This microstructured design exhibits strong potential for integration into high-power THz sources and biomedical sensing technologies that rely on optoelectronic principles.

This adaptability of these engineered structures makes them beneficial for diverse fields, enhancing the capability and performance of devices utilized in these applications. MTMs can assist sensors locate and amplify minor changes caused by weak interactions of analytes with EM stimuli [56], [57]. The label-free nature of the MTM absorber, which reduces the need for radioisotope or fluorescent labels, supports real-time, noninvasive analysis. This capability is particularly beneficial for rapid diagnosis, as it allows for the immediate and accurate detection of analytes without the complexities and potential inaccuracies introduced by labeling agents, which is crucial for early detection of several types of cancers [58], [59], [60].

The research studies proposed in [18], [19], [21], [30], [32], [59], [60], and [61] are various designs involving MTM-based absorbers at the THz range for detection of different types of cancers such as colon, cervical and skin cancers with substantial results.

The technology development and challenges in clinical validation emphasize the need for more compact and effective MTM absorbers in nano-sizes enabling nano-biosensing systems for disease detection and health monitoring [62], [63]. However, this sensor miniaturization moved the communication from low frequency ranges to higher frequencies such as THz and PHz EM waves. The research progress in MTM absorbers enabled structures to cover broader frequency ranges, i.e., from infrared (IR) to visible part of the frequency spectrum. Thus, the prospective utilization of PHz frequencies in medical sector, particularly in the diagnosis of leukemia, makes it an evolving area of research.

EM waves may undergo absorption, scattering, and reflection on interaction with tissues at PHz frequency bands. These interactions are critical in various biomedical applications, including imaging and diagnostic techniques, as they influence the way tissues respond to EM waves and thus affect the accuracy and efficacy of these methods. The waves may be absorbed by biological tissues, or may go through scattering if EM waves come across a structure within tissues [64], [65]. This scattering gives insight into microstructure and organization of tissue, which could be used for sensing or detection of disease [66]. Though, various investigations have been carried out using nanoscale MTMs at PHz frequency range for diverse applications including but not limited to sensing, imaging, energy harvesting, optical, and thermal applications [67], [68], [69], [70], [71], [72], however, not much of the research study has been found targeting biosensing for early cancer detection at the PHz frequency range. A recent study [35] introduced a nanoscale biosensor based on PHz-MTMs for the early detection of nonmelanoma skin cancer. The proposed biosensor functions as a dual-band absorber with polarization insensitivity, specifically engineered to operate within the microwave imaging (MWI) spectrum. This design offers a promising alternative to traditional diagnostic methods, enhancing detection capabilities through advanced EM absorption properties.

PHz range of frequency spectrum offers enhanced spatial resolution as compared to lower frequencies and allows label free detection, thus limiting the hazards caused due to screening agents, and as a result, process simplification is achieved [73]; however, the associated challenges like limited studies, immature technology, and necessity of a thorough understanding of PHz waves interaction with healthy and cancerous tissues prevent its substantial use in the medical field. These limitations should be addressed to absolutely leverage the ability of PHz frequency bands in biosensing and make sure dependable and effective diagnostic.

This study introduces a novel miniaturized nano-biosensor for early-stage leukemia detection, operating in the low PHz range. Key features include multiband operation, compact size, near-perfect absorption, and angle insensitivity, achieved through precise design. The sensor, with a dipole and two rings of gold or silver on a silicon dioxide ($SiO_2$) substrate, demonstrates high-performance MWI. Comprehensive simulation studies and parametric analysis validate the device's efficacy in distinguishing between healthy and cancerous samples via absorption frequency shifts. Compared to state-of-the-art biosensors, the proposed device offers superior spectral properties and spatial resolution.

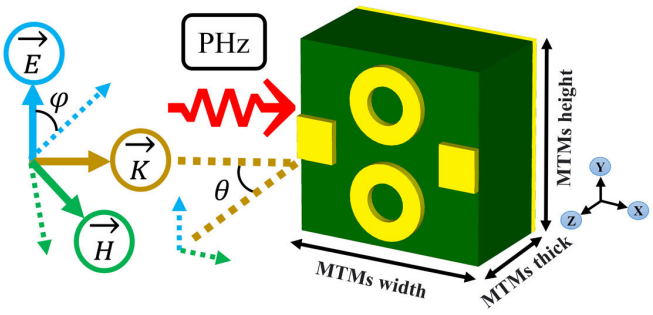


Fig. 1. Diagram of the structural design and incident field directions for a perfect absorber.

## II. Structural Design and Incident Field Orientations

The proposed biosensor employs a metal-insulator-metal (MIM) configuration, a well-established approach in plasmonic and MTM-based sensing. This structure consists of nanoscale metallic resonators positioned over an insulating layer, with a continuous metallic backplane on the opposite side. The backplane plays a critical role in suppressing wave transmission while enhancing EM interactions with the resonators. This design facilitates strong field confinement, leading to near-total absorption at the targeted resonance frequencies, thereby minimizing reflection losses and optimizing sensing performance.

A key feature of this biosensor is its function as an MTM perfect absorber (MTMPA), achieved through precise structural parameter tuning to ensure impedance matching with free space. The absorber consists of three subresonators—a dipole and two parallel rings of identical diameter—each contributing to distinct absorption peaks in the PHz range. These elements resonate at specific frequencies, generating a triple-band absorption spectrum, essential for detecting minute biological variations. The structural layout, illustrating the dipole and parallel ring resonators, is depicted in Fig. 1.

The triple-band response significantly enhances sensitivity and specificity in early-stage leukemia detection. Each absorption peak corresponds to a unique resonance mode, enabling precise identification of biomolecular changes via frequency shifts. The incorporation of multiple resonators broadens spectral response, improving diagnostic accuracy and minimizing false positives.

Fig. 1 also shows the incident field component directions used in this study together with the polarization angle and the incident angle with respect to the 3-D MTM design representation.

A wide set of structural configurations was studied and the solution components used in the final structure were highlighted as Models 1 and 2 in Fig. 2(a) and (b), respectively, for the dipole and rings. The design in Fig. 2(c) provides a

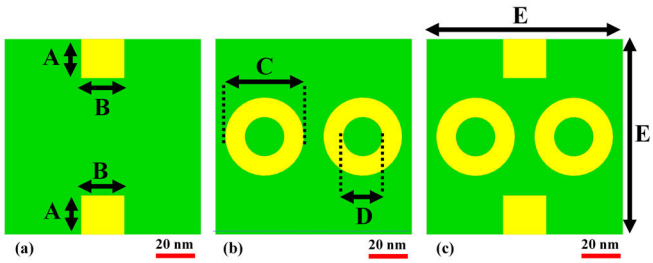


Fig. 2. Recommended designs for a perfect absorber. (a) Model 1, (b) Model 2, and (c) Model 4 (proposed biosensor design).

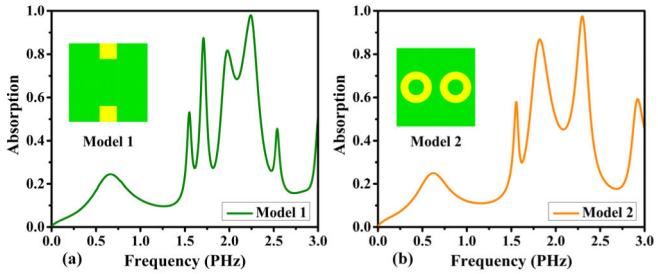


Fig. 3. Comparison of the absorption characteristics for different designs. (a) Model 1 and (b) Model 2.

TABLE I
COMPLETE LIST OF THE VARIABLES THAT HAVE BEEN ADJUSTED FOR THE RECOMMENDED SENSOR

| Parameter | Value (nm) | Parameter | Value (nm) |
|---|---|---|---|
| A | 20 | Jurkat Thick | 100 |
| B | 22 | Jurkat width | 100 |
| C | 40 | MTMs Thick | 57 |
| D | 20 | MTMs width | 100 |
| E | 100 | | |

top-view representation of the united final proposed perfect absorber.

The metal rings used in the design had a diameter of 40 nm with a central aperture of 20 nm, while the full absorber unit cell has a size of just 100 × 100 nm. Dimensions and quotas of Fig. 2 are defined in Table I, where the material thicknesses and sizes also have been specified.

The material options considered for the composition included titanium and $SiO_2$ for the insulator section, while evaluating classical good conductors such as silver and gold for the conductive reflective part.

The perfect absorber was modeled in an industry-standard CAD suite and simulated with a thin mesh approach being fine-tuned and evaluated afterward. Section III will present the main results and absorption spectra obtained for the proposed sensor device.

To ensure accurate EM field resolution and efficient computational performance, a thin mesh approach was employed in the simulation of the proposed biosensor. Given that the sensor operates in the PHz frequency range, the characteristic dimensions of the resonant structures are in the nanometer scale, necessitating precise meshing to resolve fine geometric details and field variations. Standard meshing techniques often lead to excessive computational demands due to the requirement of extremely small mesh elements across the entire simulation domain. In contrast, the thin mesh approach optimizes computational efficiency by refining the mesh specifically in regions of high field concentration, such as near the dipole and ring resonators, while maintaining sufficient accuracy in less critical areas. This method enables high-fidelity resolution of near-field interactions and ensures precise absorption characteristics at the targeted resonance frequencies.

The material properties of the biosensor were rigorously modeled using the Drude dispersion model, which accurately characterizes the optical response of metals at high-frequency regimes. The complex permittivity of the gold and silver resonators was defined as

$$\epsilon(\omega) = \epsilon_\infty - \frac{\omega_p^2}{\omega^2 + i\gamma\omega} \tag{1}$$

where $\varepsilon_\infty$ is the high-frequency permittivity, $\omega_p$ represents the plasma frequency, and $\gamma$ denotes the damping coefficient.

These parameters were extracted from experimentally validated sources to ensure realistic modeling of metal behavior in the PHz domain. Additionally, the $SiO_2$ substrate was characterized using frequency-dependent permittivity values derived from experimental data to account for its dielectric properties accurately. The interaction between the sensor's MTM elements and incident waves was analyzed using full-wave simulations, incorporating material dispersion effects to reflect real-world EM behavior.

The use of the thin mesh approach, coupled with a rigorous Drude-based material model, ensures that the numerical simulations accurately capture the biosensor's EM performance. This methodological framework enables precise prediction of resonance shifts in response to different biological samples, reinforcing the device's applicability for early-stage leukemia detection.

The optical properties of the $SiO_2$ substrate are vital for accurately modeling the biosensor's performance. In our simulations, $SiO_2$ was treated as a dielectric material with a relative permittivity ($\epsilon r$) of 3.9, which is consistent with established values for $SiO_2$ at optical frequencies within the operational range of our device (0–3 PHz). Although $SiO_2$ exhibits slight dispersion within this range, the variation in permittivity is minimal, allowing the use of a constant value for simplicity, without compromising the results' accuracy. Additionally, $SiO_2$ demonstrates extremely low loss in the PHz regime, and thus, we modeled it as a low-loss dielectric with a loss tangent ($\tan\delta$) of 0.0001. This assumption is valid due to the negligible energy dissipation in $SiO_2$ compared to the strong absorption resonances in the MTM structure. While a more complex, frequency-dependent model could enhance precision, the simplified approach balances computational efficiency and accuracy, effectively capturing the sensor's key operating physics.

## III. ABSORPTION PROPERTIES AND CHARACTERISTICS

The perfect absorber will be addressed using a constructive approach evaluating its building structures and afterward joining them as shown for the proposed structure, illustrating the path used to design and tune the device.

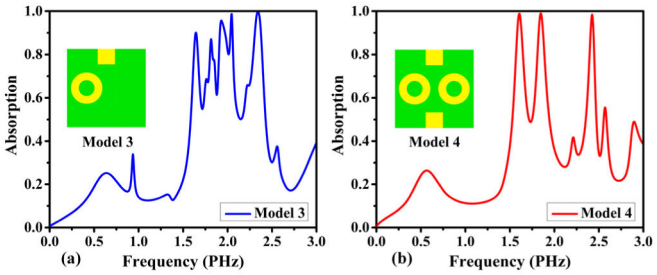


Fig. 4. Comparison of absorption properties for various designs. (a) Model 3 and (b) Model 4.

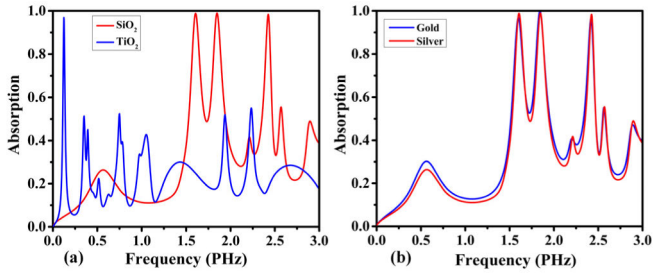


Fig. 5. Absorption spectra for the proposed design under varying conditions. (a) Substrate material and (b) resonator material.

The simulations were targeted in the low PHz frequency range and several absorption profiles will be used to show and understand the behavior of the absorbers, it was chosen to simulate up to the frequency of 3 THz in most of the graphs as it covers well the application range. The analysis starts with Fig. 3(a) where the Model 1 design post-tune results are shown.

The absorption profile of Model 1 shows two high absorption peaks being the highest near 2.4 PHz, the results are promising but the peaks are not as high as similar works already studied for the case. There is also a lack of sensitivity in the second peak, which is not fully adequate for the application.

Due to these limitations in Model 1, other options were studied and the dual ring structure named Model 2 was developed. Fig. 3(b) shows the results for this model.

This version also shows two high absorption peaks, one at 1.8 PHz and another near 2.4 PHz, both ones with better selectivity than the previous case, but this time, the first peak is not as sharp as the previous case and also it did not reach near to one absorption value.

The single-typed structure options researched and studied did not achieve absorption profiles as near as perfect absorption as intended and the targeted triple band approach was not reached with these. As a next step to the solution, a mix of Models 1 and 2 half sections was adjusted to provide at least the three desired peaks with good absorption, Fig. 4(a) shows the obtained device, named Model 3 together with its absorption spectrum.

The absorption profile of Model 3 has improved absorption values with respect to the previous studies and partially achieved the multiband desired characteristics. In contrast, the first absorption peak was not as high as the others, there is a section with several spurious peaks and there is also a lack of specificity in the middle band.

The final design step was to add symmetry to the structure achieving an absorber similar to the joined Models 1 and 2 versions, this design was named Model 4.

Fig. 4(b) shows the absorption spectral distribution for the final Model 4 design. The curve shows three absorption peaks at 1.605, 1.848, and 2.424 PHz, being all of them very sharp and isolated providing good selectivity.

All three peaks had near unitary absorption and with these results, the Model can be stated as a triple band perfect absorber, which was selected as the proposed design to be used as the nano-biosensor in this application. Section IV addresses the internal field interactions in the achieved MTM.

The proposed nano-biosensor employs a triple-band MTMPA architecture, integrating a dipole and two parallel, identical-diameter metallic rings on a $SiO_2$ substrate with a metallic backplane. Through impedance matching and localized field enhancement, the structure achieves near-unity absorption at PHz frequencies, leveraging high photon energy and short wavelengths to enhance biomolecular interactions and sensitivity. The sensor's compact design facilitates integration into lab-on-a-chip and implantable platforms, while its angle-insensitive response ensures operational robustness in practical imaging systems. Frequency shift detection enables precise discrimination of biomolecular variations, positioning the sensor as a next-generation tool for high-sensitivity diagnostics. Full-wave EM simulations validate its absorption properties, underscoring the pivotal role of computational modeling in MTM-based sensor optimization. This study establishes a foundational framework for advanced multifrequency biosensing applications, particularly for early-stage leukemia detection.

The selection of the 0–3 PHz frequency range, particularly the resonant frequencies at 1.61, 1.85, and 2.42 PHz, is based on their critical role in enhancing the biosensor's sensitivity to biomolecular changes associated with leukemia. This frequency range encompasses the visible spectrum and extends into both the IR and ultraviolet (UV) regions, where EM waves interact strongly with biological matter. The ability of EM radiation to induce molecular vibrations, rotational transitions, and electronic excitations in this range makes it highly suitable for biosensing applications.

The proposed biosensor operates by exploiting strong localized EM field enhancements at the selected resonant frequencies. These enhanced fields significantly amplify the interaction between incident radiation and biological samples, making the sensor highly responsive to even minute variations in dielectric properties. This heightened sensitivity enables precise detection of subtle changes in biomolecular composition, such as those associated with leukemic cells, leading to a measurable shift in resonance frequency. The strong field confinement and enhanced absorption at these resonances contribute to the sensor's exceptional detection capabilities.

Furthermore, the use of a triple-band resonance strategy significantly improves the biosensor's sensitivity and specificity. Each of the selected resonant frequencies interacts uniquely with biological molecules, providing complementary informa-

tion about the sample. This multiband approach reduces the likelihood of false positives and enhances detection accuracy, as different biomolecular structures exhibit distinct responses at different frequencies. While exact biomolecular spectral signatures in the PHz regime are still an area of active research, the selected frequencies align well with known molecular vibrational modes, electronic transitions, and light-matter interactions relevant to biosensing.

The precise selection of these resonances was determined through rigorous full-wave EM simulations and structural optimization. The sensor's MTM-based design was fine-tuned to achieve near-perfect absorption at the target frequencies, maximizing its sensitivity to variations in biological samples. These design choices ensure that the biosensor is capable of detecting early-stage leukemia with high accuracy and reliability. By leveraging strong resonant field enhancements and an optimized multiband configuration, the proposed sensor offers a significant advancement in the field of optical biosensing.

## IV. EM Response and Field Distribution Analysis

This section comprehensively analyzes the EM response and field distribution of the MTM-based biosensor. It covers material and geometrical optimization, examines material properties including RI, and presents detailed visualizations of $E$- and $H$-field distributions. Additionally, it explores surface current distributions and angular dependence of absorption, providing insights for optimizing the biosensor's design and performance in detecting EM interactions.

### A. Material and Geometrical Optimization

The performance and functionality of a biosensor depend heavily on the choice of materials used in its construction. In this study, silver (Ag) and gold (Au) were selected for the conductive reflective layer, while titanium dioxide ($TiO_2$) and $SiO_2$ were chosen as the insulating materials. Each material was carefully selected to balance electrical, optical, and biological properties, optimizing the biosensor's performance for early-stage leukemia detection.

Silver and gold were selected as the conductive elements due to their exceptional electrical conductivity, biocompatibility, and stability. Silver, with its highest electrical conductivity among metals, ensures minimal ohmic losses, thereby enhancing the plasmonic efficiency and EM field confinement. This is critical for maximizing the sensor's sensitivity and absorption performance at the targeted frequencies. Gold, in contrast, offers remarkable chemical stability and resistance to oxidation, ensuring long-term reliability and maintaining the sensor's performance over time. Additionally, gold facilitates the immobilization of biomolecules, preserving their biological activity and enhancing the sensor's specificity for detecting leukemia biomarkers.

The insulating layer of the biosensor is composed of $TiO_2$ and $SiO_2$. $TiO_2$ is a highly biocompatible, chemically stable, and nontoxic material, offering high dielectric properties and enabling efficient electron transfer between the sensor and biomolecules. $TiO_2$ nanostructures also provide a high surface-to-volume ratio, improving surface reaction activity and enhancing biomolecule adsorption. $SiO_2$, with its excellent insulating properties and transparency in the PHz range, ensures signal integrity and minimizes interference. Additionally, $SiO_2$'s compatibility with semiconductor fabrication processes makes it an ideal choice for the fabrication of miniaturized, high-performance biosensors.

The careful selection of these materials, combining the high conductivity of silver and gold with the superior dielectric properties of $TiO_2$ and $SiO_2$, ensures that the proposed biosensor achieves high sensitivity, minimal signal loss, and stable performance. These material choices provide a robust platform for early-stage leukemia detection, enabling the biosensor to operate with high spatial resolution and discriminate subtle changes in biomolecular signatures with remarkable accuracy.

The absorption properties of the proposed biosensor are dictated by the EM characteristics of its constituent materials, including permittivity, permeability, and conductivity. In MTM-based structures, absorption arises from interactions between incident EM waves and resonant elements, leading to energy dissipation through electronic transitions, lattice vibrations, and plasmonic excitations. The substrate material critically influences absorption efficiency and spectral response. In this study, $SiO_2$ and $TiO_2$ are chosen for their distinct optical and dielectric properties, which govern their absorption behavior.

$SiO_2$, with a wide bandgap of approximately 8.9 eV, supports broad absorption across multiple frequencies. Its amorphous structure facilitates diverse photon interactions, resulting in a continuous absorption spectrum. Additionally, its stable lattice and low defect density contribute to consistent optical performance, reducing energy dissipation losses and making it highly suitable for multiband biosensing applications.

$TiO_2$, particularly in its anatase and rutile phases, exhibits strong absorption in the UV region due to its lower bandgap ($\sim$3.0 eV) and excitonic effects. However, its absorption properties are highly dependent on crystallinity and defect density, which influence its effective permittivity. These variations underscore the importance of precise material selection in optimizing biosensor performance for specific spectral applications.

EM response and field distribution analysis is a crucial aspect of studying EM fields and their interactions with different materials or structures. It involves analyzing how EM waves propagate, absorb, or refract when interacting with media. The distribution of electric and magnetic fields in a given space is essential for understanding the behavior of EM waves and designing devices such as antennas, waveguides, and transmission lines. Various techniques can be used for EM response and field distribution analysis, including finite element analysis (FEA), finite difference time domain (FDTD) method, and finite element method (FEM). These methods help engineers and researchers simulate and visualize the EM fields in different scenarios, allowing for optimizations and improvements in design and performance. Overall, EM response and field distribution analysis play a critical role in the development of various technologies, from communications systems to radar systems, medical devices, and more.

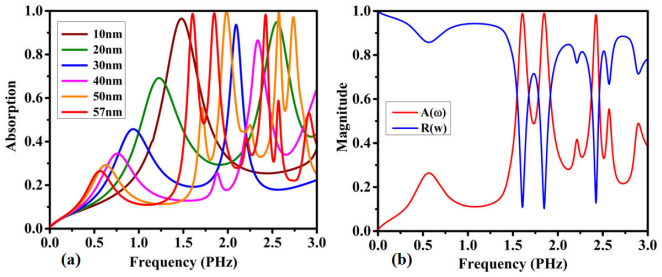


Fig. 6. (a) Impact of substrate thickness on absorption capability. (b) Reflection and absorption spectra of the absorber.

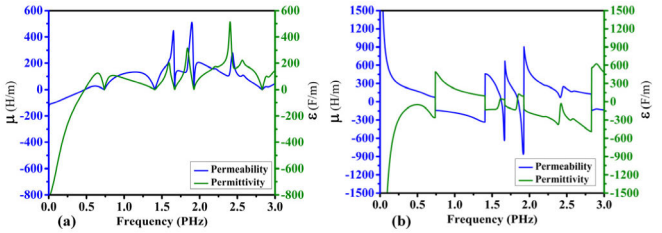


Fig. 7. Real and imaginary components of permeability ($\mu$) and permittivity ($\varepsilon$) for the proposed absorber. (a) Real components of $\mu$ and $\varepsilon$. (b) Imaginary components of $\mu$ and $\varepsilon$.

Conducting these analyses helps ensure the efficient operation and functionality of EM devices and systems. Here, absorption spectrum is used for both parts of the structure: a) substrate and b) resonator. As can be seen in Fig. 5, absorption is calculated in the range of 0–3 PHz. In Fig. 5(a), the absorption is shown for $SiO_2$ and $TiO_2$. It is clear that in three frequencies perfect absorption is available for $SiO_2$. In contrast, in $TiO_2$, near-perfect absorption in single frequency is occurred. Absorption spectrum for resonator materials including gold and silver is calculated in Fig. 5(b) and similar results are obtained for both materials.

The influence of substrate thickness on the absorption characteristics of the proposed nano-biosensor was systematically investigated through full-wave simulations, with thickness variations ranging from 10 to 57 $\mu$m. The results, depicted in Fig. 6(a), reveal a distinct correlation between the substrate thickness and the number of resonance modes. For thicknesses between 10 and 40 $\mu$m, the biosensor exhibits a single absorption peak with an efficiency of approximately 90%. This behavior arises from the limited interaction volume within the $SiO_2$ substrate, which restricts the formation of additional resonant modes. The confined EM field interaction at these lower thicknesses supports only a fundamental resonance mode, resulting in a single absorption peak.

However, as the substrate thickness increases to 50 $\mu$m, a transition to a triple-band resonance response is observed. This shift can be attributed to the increased optical path length, which enhances phase accumulation and promotes additional resonant modes within the MTM structure. The increased substrate thickness facilitates stronger coupling between the incident EM waves and the resonating metallic elements, leading to the excitation of multiple resonance modes. This transition is a direct consequence of the enhanced field confinement and impedance matching conditions, which optimize energy coupling into the structure. The emergence of multiple resonance points significantly enhances the spectral resolution of the sensor, making it more effective in detecting subtle biomolecular changes associated with early-stage leukemia.

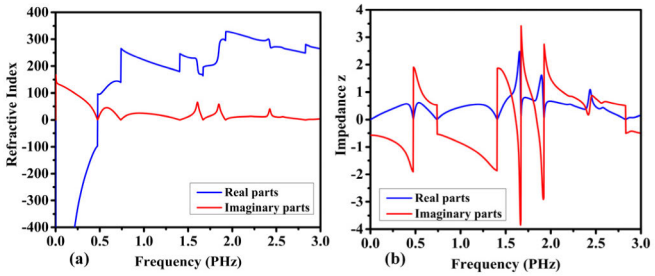


Fig. 8. Simulated parameter responses of the proposed model. (a) Real and imaginary parts of the RI. (b) Impedance (z).

The reflection and absorption spectra of the biosensor, as illustrated in Fig. 6(b), further validate the impact of substrate thickness on the device's EM response. The optimized biosensor, with a substrate thickness of 57 $\mu$m, exhibits near-unity absorption at multiple resonance frequencies while maintaining minimal reflection. This behavior is indicative of strong impedance matching between the MTM structure and the surrounding medium, which minimizes reflection losses and maximizes energy absorption. The presence of distinct triple-band absorption further confirms the critical role of substrate thickness in tuning the resonant characteristics of the biosensor.

The observed reduction in reflection across these resonance frequencies underscores the efficiency of the proposed structure in localizing and enhancing the EM field within the sensing region. This field enhancement is crucial for achieving high sensitivity, as it amplifies the interaction between the incident waves and the targeted biomolecular samples. By leveraging a multiresonance response, the biosensor ensures precise discrimination between healthy and cancerous samples, thereby improving diagnostic accuracy and reliability.

### B. Material Properties and RI

The real and imaginary components of permeability ($\mu$) and permittivity ($\varepsilon$) for the proposed absorber can vary depending on the material used and the frequency of operation. In general, the real component of permeability represents the material's ability to support magnetic fields, while the imaginary component accounts for any losses in the material. Similarly, the real component of permittivity [Fig. 7(a)] describes the material's ability to store electrical energy, while the imaginary component [Fig. 7(b)] accounts for losses in the material. For an absorber, it is important to have high imaginary components of both permeability and permittivity to efficiently absorb EM waves. By tuning these parameters, the absorber can be optimized for specific frequencies and applications.

So, here, real and imaginary parts of the absorber are calculated as frequency is changed from 0 to 3 PHz. In agreement to Fig. 5, three points can be used for perfect absorber.

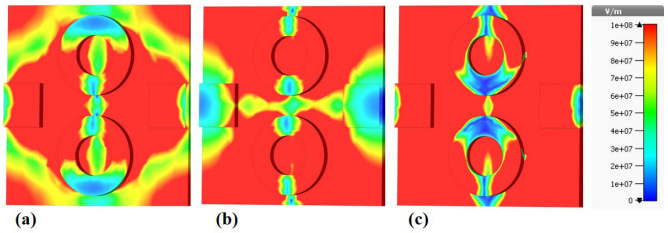


Fig. 9. Visualization of the real components of the/*E*/-field distributions in the MTM structure at (a) 1.605 PHz, (b) 1.848 PHz, and (c) 2.424 PHz.

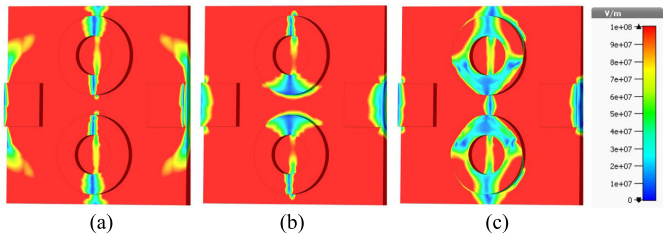


Fig. 10. Visualization of the imaginary components of the /*E*/-field distributions in the MTM structure at (a) 1.605 PHz, (b) 1.848 PHz, and (c) 2.424 PHz.

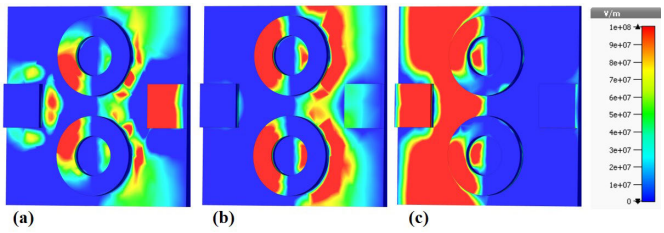


Fig. 11. Visualization of the real components of the *Ez*-field distributions in the MTM structure at (a) 1.605 PHz, (b) 1.848 PHz, and (c) 2.424 PHz.

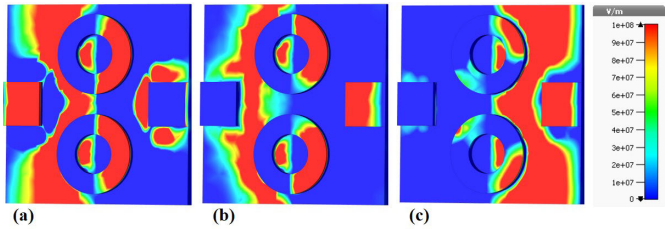


Fig. 12. Visualization of the imaginary components of the *Ez*-field distributions in the MTM structure at (a) 1.605 PHz, (b) 1.848 PHz, and (c) 2.424 PHz.

The real part of the RI, also known as the ordinary index of refraction, is a measure of how much light slows down as it enters a medium compared to its speed in a vacuum. The imaginary part of the RI, also known as the extinction coefficient, represents the absorption of light as it passes through a medium. Together, these two components describe how light interacts with matter and are essential in understanding the behavior of EM waves in different mediums.

So, to further investigate the performance of the absorber, we have also inspected the real and imaginary parts of RI of the structure when frequency increases from 0 to 3 PHz in Fig. 8(a). Also, to gain more details about the behavior of the absorber impedance is calculated in Fig. 8(b).

### C. Electric Field Distributions

Figs. 9 and 10 collectively illustrate the real and imaginary components of the electric field ($E$-field) distributions within an MTM-based biosensor, respectively. These visualizations at three specific frequencies—1.605, 1.848, and 2.424 PHz—provide comprehensive insights into the sensor's EM response characteristics.

In Fig. 9, the real components of the $E$-field distributions are displayed. At 1.605 PHz [Fig. 9(a)], the high-intensity regions surrounding the circular structures indicate strong field localization, pointing to a resonant interaction at this frequency. This is essential for enhancing the sensor's sensitivity. At 1.848 PHz [Fig. 9(b)], the $E$-field distribution shifts to pronounced intensity along the central axis and periphery of the circles, suggesting a different resonant mode. At 2.424 PHz [Fig. 9(c)], the high-intensity regions predominantly around the outer edges of the circles indicate another distinct resonance, confirming the sensor's capability to operate across multiple frequency bands.

Fig. 10, in contrast, presents the imaginary components of the $E$-field distributions. At 1.605 PHz [Fig. 10(a)], the concentrated intensity along the central vertical axis and edges of the circular resonators suggests significant energy dissipation, characteristic of resonant absorption. This is a hallmark of the MTM's ability to effectively absorb EM waves at specific frequencies. At 1.848 PHz [Fig. 10(b)], the high-intensity regions in the horizontal plane and around the outer edges of the circles reveal a different pattern of energy dissipation, indicating the presence of another resonant mode. At 2.424 PHz [Fig. 10(c)], the complex distribution with intense fields around the larger circular structures and along the central axis signifies the third resonance peak.

Contrasting Figs. 9 and 10, the real components of the $E$-field (Fig. 9) primarily indicate where the electric field is strongest, which corresponds to regions of high sensitivity and potential signal enhancement. These are the areas where the sensor can most effectively detect changes in its environment. The imaginary components (Fig. 10), however, reflect the areas of energy dissipation and loss within the sensor. These are crucial for understanding the MTM's absorptive properties and how it converts incident EM energy into other forms, such as heat.

The contrasting patterns observed in Figs. 9 and 10 at the three frequencies underscore the MTM's multiband functionality and its suitability for applications requiring precise EM wave manipulation.

In Fig. 11, which illustrates the real components of the $Ez$-field, the distributions reveal where the electric field is strongest in terms of the actual energy flowthrough the MTM structure. At 1.605 PHz [Fig. 11(a)], high-intensity regions are localized around the circular resonators and the central bar structure, indicating strong interaction and energy transfer at these points. As the frequency increases to 1.848 PHz [Fig. 11(b)], these high-intensity areas expand and reconfigure, suggesting changes in the resonance behavior and energy distribution within the MTM. At 2.424 PHz [Fig. 11(c)], the high-intensity regions become even more extensive, showing a broadening of the energy transfer

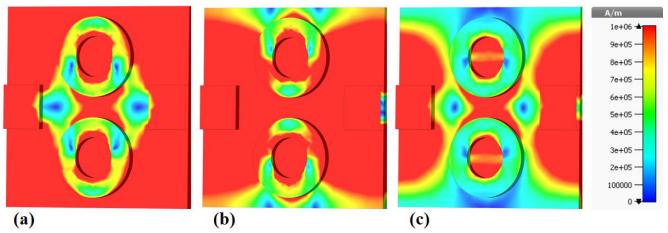


Fig. 13. Visualization of the real components of the /*H*/-field distributions in the MTM structure at (a) 1.605 PHz, (b) 1.848 PHz, and (c) 2.424 PHz.

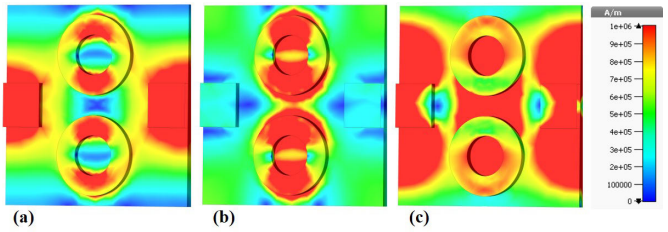


Fig. 14. Visualization of the imaginary components of the /*H*/-field distributions in the MTM structure at (a) 1.605 PHz, (b) 1.848 PHz, and (c) 2.424 PHz.

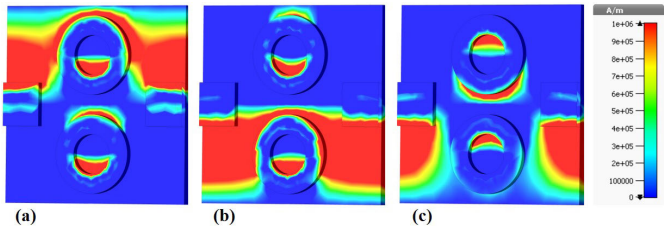


Fig. 15. Visualization of the real components of the *Hz*-field distributions in the MTM structure at (a) 1.605 PHz, (b) 1.848 PHz, and (c) 2.424 PHz.

pathways within the structure. These patterns highlight the frequency-dependent nature of the energy interaction with the biosensor's components.

Contrastingly, Fig. 12 presents the imaginary components of the $Ez$-field distributions, which are associated with the reactive power and energy storage within the MTM. The imaginary component indicates the phase lag between the electric field and the induced polarization, which is critical for understanding the absorptive properties of the material. At 1.605 PHz [Fig. 12(a)], the high-intensity imaginary $Ez$-field regions are also concentrated around the circular resonators and the central bar, suggesting significant energy storage in these areas. As the frequency rises to 1.848 PHz [Fig. 12(b)], the distribution shifts, with high-intensity regions becoming more pronounced near the inner edges of the circular resonators, indicating a change in how the energy is stored reactively within the structure. At 2.424 PHz [Fig. 12(c)], the high-intensity imaginary $Ez$-field regions cover a more extensive area along the horizontal axis intersecting the resonators, further emphasizing the strong reactive component at this frequency.

The comparison between Figs. 11 and 12 reveals the distinct roles played by the real and imaginary components of the electric field in the biosensor's operation. While the real component (Fig. 11) highlights the areas of strong energy

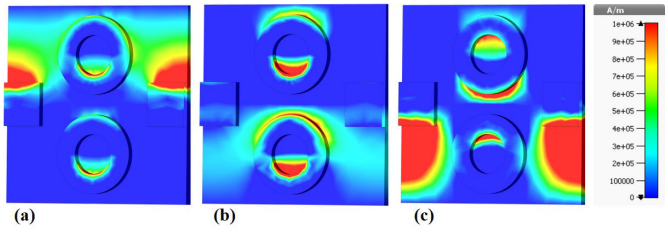


Fig. 16. Visualization of the imaginary components of the *Hz*-field distributions in the MTM structure at (a) 1.605 PHz, (b) 1.848 PHz, and (c) 2.424 PHz.

flow and direct interaction with the EM waves, the imaginary component (Fig. 12) underscores the regions where energy is stored and phase lag occurs. Together, these figures provide a comprehensive understanding of the electric field dynamics within the MTM structure, elucidating how the biosensor achieves its triple-band absorption and enhances its sensitivity and specificity for detecting target analytes. The interplay between the real and imaginary components across different frequencies is crucial for optimizing the design and functionality of the MTM perfect absorber.

### D. Magnetic Field Distributions

In Fig. 13, the real components of the magnetic field ($H$-field) provide insight into the actual magnetic field intensity and distribution within the MTM structure. At 1.605 PHz [Fig. 13(a)], the field is highly localized around the inner and outer edges of the circular resonators, indicating strong magnetic resonances. This pattern suggests that the MTM is efficiently coupling with the incident EM waves, resulting in high field intensities. Similarly, at 1.848 PHz [Fig. 13(b)] and 2.424 PHz [Fig. 13(c)], the $H$-field distributions change, reflecting different resonant modes. These variations in field patterns are crucial for understanding how the structure supports multiple resonant frequencies, each characterized by distinct EM interactions.

In contrast, Fig. 14 shows the imaginary components of the $H$-field, which are essential for understanding the energy dissipation and reactive power within the MTM. At 1.605 PHz [Fig. 14(a)], the imaginary $H$-field distribution also concentrates around the edges of the resonators but in a pattern that indicates the phase lag between the magnetic field and the current in the structure. This phase information is critical for analyzing the reactive energy storage in the MTM. At 1.848 PHz [Fig. 14(b)] and 2.424 PHz [Fig. 14(c)], the imaginary $H$-field distributions change, illustrating how the energy dissipation and storage mechanisms differ across the resonant frequencies.

The comparison between Figs. 13 and 14 highlights the complementary nature of the real and imaginary $H$-field components. The real components (Fig. 13) reflect the actual magnetic field intensity and spatial distribution, which are directly related to the sensor's interaction with external EM waves. These patterns indicate where the strongest interactions and resonances occur within the MTM structure. In contrast, the imaginary components (Fig. 14) reveal the energy dissipation and storage characteristics, providing insight into the reactive power and loss mechanisms within the sensor.

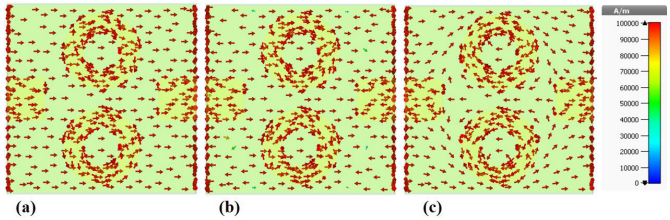


Fig. 17. Visualization of the real components of the surface current distributions in the MTM structure at (a) 1.605 PHz, (b) 1.848 PHz, and (c) 2.424 PHz.

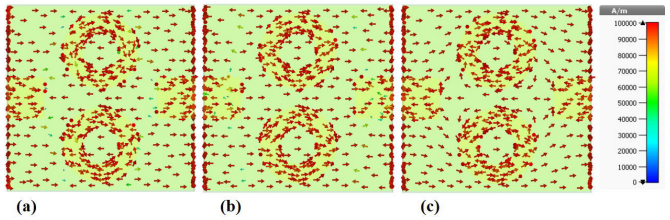


Fig. 18. Visualization of the imaginary components of the surface current distributions in the MTM structure at (a) 1.605 PHz, (b) 1.848 PHz, and (c) 2.424 PHz.

Understanding both the real and imaginary components is essential for optimizing the performance of the biosensor. The real $H$-field distributions help identify the regions of maximum field enhancement, which are critical for detecting biological analytes. The imaginary $H$-field distributions, meanwhile, provide information on how energy is stored and dissipated, which is vital for minimizing losses and improving the sensor's sensitivity and efficiency. Together, these components offer a comprehensive picture of the EM behavior of the MTM perfect absorber, guiding the design and optimization of high-performance biosensors.

Fig. 15 illustrates the real components of the $Hz$-field distributions in an MTM-based biosensor at frequencies 1.605, 1.848, and 2.424 PHz. The magnetic field intensity ranges from 0 to $1e^{+6}$ A/m, providing a clear view of the magnetic resonance behavior at these frequencies. The distributions reveal a significant concentration of magnetic fields within and around the circular resonators, highlighting the regions of maximum magnetic field interaction and absorption. The real components give insight into the spatial distribution of the magnetic fields and show how the structure interacts with the external magnetic field in real-time.

In contrast, Fig. 16 presents the imaginary components of the $Hz$-field distributions at the same frequencies. These imaginary components are critical for understanding the phase-related characteristics of the magnetic fields. The imaginary parts represent the stored energy in the resonator system and indicate how the fields oscillate and dissipate energy over time. This phase information is essential for analyzing the loss mechanisms and resonance quality of the MTM structure.

At 1.605 PHz, both figures show a concentration of magnetic fields around the resonators, but Fig. 15(a) highlights the immediate magnetic response, whereas Fig. 16(a) focuses on the oscillatory behavior and energy storage. This difference is crucial as it illustrates not just where the fields are strongest but how they behave dynamically within the structure.

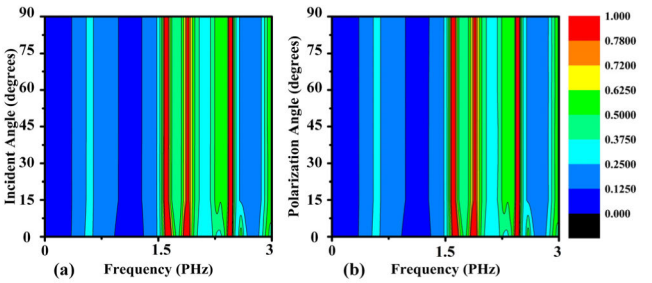


Fig. 19. Investigation of the impact of angle modification on absorption rate for (a) incidence angle and (b) polarization angle.

At 1.848 PHz, the real components in Fig. 15(b) exhibit stronger field intensities, indicating a robust interaction with the resonators. The imaginary components in Fig. 16(b), on the other hand, show how this interaction translates into energy storage and dissipation, which are key for understanding the efficiency and effectiveness of the biosensor's resonance.

At 2.424 PHz, the field distributions in both figures [Figs. 15(c) and 16(c)] show increased complexity and intensity. The real components reveal the expanded reach of the magnetic fields within the resonators, while the imaginary components provide detailed information on the phase shifts and energy loss, giving a complete picture of the biosensor's performance at this higher frequency.

### E. Surface Current Distributions and Angular Dependence of Absorption

The absorption behavior of the proposed model is easily understood based on electric field distribution. The analysis of the proposed design carried out for the real and imaginary components for different resonating frequencies of 1.605, 1.848, and 2.424 PHz is shown in Figs. 17 and 18. It is very clear that in both real and imaginary components the current distribution is rotating in a clockwise direction and focusing toward the centered located resonators. The high concentration is also visualized in real and imaginary components.

The effect of absorption by changing the incident angle is observed in Fig. 19(a), and the polarization angle effect of absorption is shown in Fig. 19(b). It is very clear that between 1.5 and 2.5 PHz spectrum absorption rate does not affect angle variation. The same vertical color represents no effect on effect on absorption by the changing angle. Based upon the response it is clear that sensing-based applications are supported by the proposed model.

The observed insensitivity of the proposed biosensor's absorption rate (between 1.5 and 2.5 PHz) to variations in incident and polarization angles is a deliberate design choice aimed at enhancing the robustness and reliability of the device. This angular stability ensures consistent performance across a range of illumination conditions, a critical requirement for practical applications, particularly in clinical diagnostics where precise alignment may be challenging. By decoupling the sensor's response from minor variations in incident wave direction, we minimize a potential source of measurement error and improve the reliability of the detected signal.

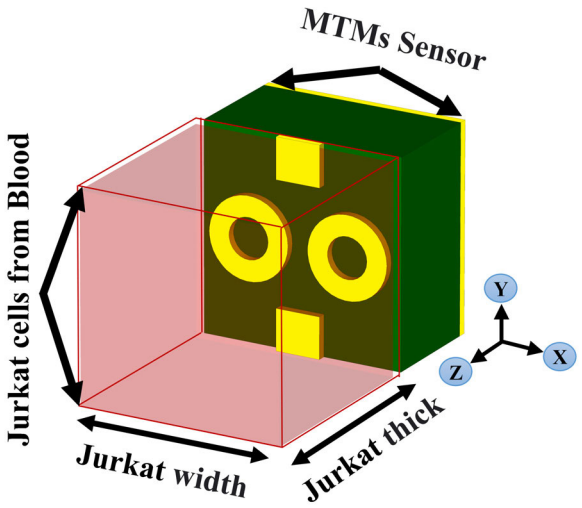


Fig. 20. Analysis of the absorption coefficient of the proposed biosensor in both healthy blood and blood affected by cancer.

It is crucial to distinguish between the incident angle of the EM wave and the orientation of the sensor relative to the biological tissue. While our sensor is designed to be insensitive to the former, we fully acknowledge the diagnostic value of controlled variations in the latter. Different viewing angles can indeed provide complementary information about the tissue's structure and composition, a principle exploited in techniques like tomography. Therefore, the angle insensitivity of the sensor itself should not be interpreted as a preclusion of multiangle measurements; rather, it simplifies the design and interpretation of such measurements.

The inherent angular stability of our biosensor allows for a more straightforward implementation of multiangle diagnostic protocols. Clinicians can strategically adjust the sensor's orientation to acquire data from multiple perspectives without the confounding factor of the sensor's own response varying with incident angle. This decoupling of sensor response from incident angle variations enhances the accuracy and interpretability of multiangle data. Future study will focus on integrating this sensor into a system capable of precise and controlled manipulation of sensor orientation, enabling the exploration of multiangle diagnostic strategies for improved tissue characterization. This will involve investigating mechanical or robotic systems for automated angular adjustments, combined with advanced signal processing techniques to reconstruct detailed information about the tissue under examination.

Furthermore, the concern regarding rigidity in the sensor's response due to angle insensitivity overlooks the fundamental principle of operation: detection relies on frequency shifts induced by the sample, not direct measurement of the incident angle. The sensor's inherent insensitivity to the incident wave angle serves to stabilize the baseline response, allowing for more reliable detection of these subtle frequency shifts. The complex dielectric landscape of the biological material, with its inherent heterogeneity, directly influences the EM field surrounding the sensor, resulting in unique frequency shift patterns. These patterns, rather than the incident angle itself, encode the information about the sample's composition and structure. Our simulations, employing realistic models of healthy and cancerous blood, demonstrate the detectability of these shifts despite the sensor's angle-insensitive nature, validating its capacity to discern variations within complex biological matrices.

It is also important to emphasize that angle insensitivity does not preclude the use of multiangle measurements; on the contrary, it enhances their interpretability. By providing a stable baseline, our sensor facilitates the extraction of meaningful information from multiangle data, as variations in the measured signal can be more confidently attributed to the sample's properties rather than fluctuations in the sensor's inherent response. Future study will explore the integration of this sensor with precisely controlled manipulation systems to fully leverage the diagnostic potential of multiangle interrogation, combining the sensor's stability with the rich information accessible through varied perspectives of the biological sample. This combination of intrinsic angle insensitivity with controlled extrinsic angle variation promises to unlock a more nuanced understanding of complex biological systems.

## V. Optimization of Resonant Frequencies for Leukemia Detection

The selection of resonant frequencies in biosensors is critical for achieving high sensitivity and specificity in disease detection. In this study, the chosen frequencies (1.605, 1.848, and 2.424 PHz) were systematically optimized to target distinct EM signatures associated with leukemia. These frequencies correspond to points of maximal field enhancement and near-perfect absorption, ensuring precise detection of subtle dielectric variations induced by leukemic cells.

While biological tissues interact with a broad spectral range, not all frequencies contribute equally to diagnostic accuracy. The sensor's triple-band design enhances detection reliability by providing internal validation across multiple resonances, minimizing false positives, and improving diagnostic confidence. Expanding the frequency range beyond these optimized points would not necessarily improve sensitivity, as the selected frequencies are already optimized for maximum interaction with leukemia biomarkers.

This sensor is designed as a specialized diagnostic tool within a broader biomedical framework, complementing other diagnostic techniques. Its targeted frequency selection ensures efficient, high-precision detection, reinforcing the validity of its design without the need for additional spectral analysis.

## VI. Specificity and Reliability of the Proposed Biosensor

Ensuring the specificity and reliability of the proposed biosensor is essential for its effectiveness in leukemia detection. The dielectric properties of biological tissues vary significantly between healthy and malignant states due to differences in cellular structure, membrane conductivity, and metabolic activity. To accurately distinguish leukemia from normal blood, we utilized Jurkat cells, a well-established model in leukemia research, within our simulations. The unique EM signature of Jurkat cells enables differentiation

from normal blood components, reducing the risk of false detections arising from other hematological conditions.

Our approach focuses on detecting leukemia-specific dielectric property variations rather than general alterations in blood composition. Since Jurkat cells are widely used as a benchmark in leukemia studies, their incorporation into our simulation framework ensures that the biosensor is tuned to recognize leukemia-specific EM changes. This methodology enhances detection accuracy and minimizes the likelihood of false positives caused by normal physiological variations or other blood disorders.

To further validate the specificity of our biosensor, we conducted a comparative dielectric property analysis between Jurkat cells and normal blood samples within the simulation framework. The results indicate a distinct resonance shift in response to leukemic cells, which is absent in healthy blood samples. This confirms that the proposed sensor effectively differentiates between leukemic and nonleukemic conditions based on dielectric signature variations.

While our simulation results demonstrate high specificity, additional in vitro and in vivo studies will be necessary to confirm the sensor's real-world performance. The complexity of biological environments introduces potential interferents, such as other blood disorders with overlapping dielectric properties. Future experimental validation will be crucial to ensure the biosensor's diagnostic precision under clinically relevant conditions. Nevertheless, the findings presented in this study establish a strong foundation for the sensor's potential application in early leukemia detection.

## VII. Blood Cancer Diagnosis

The groundbreaking leukemia diagnostic biosensor utilizes advanced technology, specifically MWI, to detect and diagnose leukemia in its early stages. MWI functions by transmitting microwave signals through biological tissues and analyzing how these signals are transmitted and absorbed. Cancerous cells possess different electrical properties than healthy cells, influencing their interaction with microwave signals. Through precise modeling and measurement of these interactions, the biosensor can efficiently identify the presence of leukemia cells. This technology is a significant advancement in medical diagnostics as it tackles various challenges. Conventional methods of leukemia diagnosis can be time-consuming and may fail to detect the disease until it has advanced. Early detection is vital for effective treatment and enhancing patient outcomes. The biosensor's capability to swiftly and accurately pinpoint cancer cells suggests that it could potentially result in earlier interventions. By utilizing MWI, the leukemia diagnostic biosensor presents a promising solution to enhance the speed and precision of leukemia diagnosis. This innovation has the potential to improve patient diagnoses by enabling early detection and treatment of the disease. The proposed technique for detecting leukemia utilizes a sensor capable of differentiating between the refractive indices of healthy blood and leukemia-affected blood. The setup, as depicted in Fig. 20, consists of two coverslips with a blood sample containing Jurkat cells, which are indicative of leukemia, placed in between. This approach ensures precise outcomes

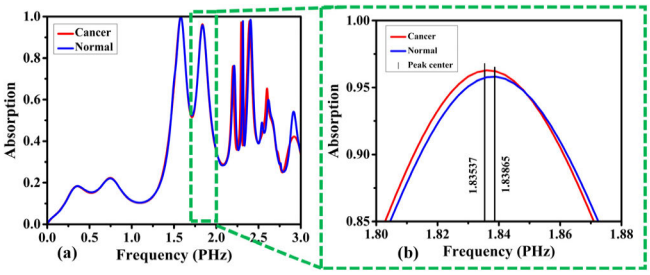


Fig. 21. Detection of absorption coefficients by the proposed biosensor for normal blood and blood cancer within the frequency range of (a) 0–3 PHz and (b) 1.8–1.88 PHz.

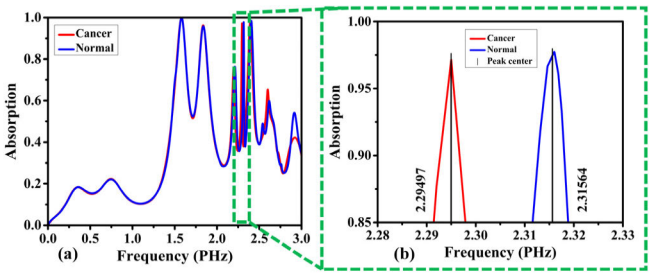


Fig. 22. Detection of absorption coefficients by the proposed biosensor for normal blood and blood cancer within the frequency range of (a) 0–3 PHz and (b) 2.28–2.33 PHz.

by maintaining a controlled environment for the sample. By analyzing the distinct refractive indices, the sensor is able to distinguish between healthy blood (with an RI of 1.376) and leukemia-affected blood (with an RI of 1.39) [24], [74], [75], [76], [77], [78]. The significant variation in RI enables accurate diagnosis. The effectiveness of this method lies in its capability to detect these minute RI changes, thereby offering a dependable and noninvasive diagnostic tool for leukemia.

Fig. 21(a) illustrates the results of the examination conducted on healthy and cancerous blood cells. The focus of the analysis was primarily on the initial peak within the frequency range of 1.5–2 PHz for both conditions. Conversely, Fig. 21(b) highlights a significant difference between healthy and cancerous blood samples, with a variation of 0.00328 PHz, ranging from 1.83537 to 1.83865 PHz. This difference demonstrates the potential of PHz imaging in detecting subtle changes in blood composition.

Fig. 22(a) displays the examination results of healthy and cancerous blood cells, specifically focusing on the second peak within the frequency range of 2–2.5 PHz for both blood conditions. Fig. 22(b) emphasizes a significant difference between healthy and cancerous blood samples, showcasing a variation of 0.02067 PHz, from 2.29497 to 2.31564 PHz.

Fig. 23(a) displays the detection outcomes of healthy and cancerous blood cells. The primary objective of the investigation was to compare healthy and cancerous blood cells within the 2–3 PHz range at the third peak. In Fig. 23(b), there is a notable contrast between healthy and cancerous blood cells, with a discernible variance of 0.01174 PHz, ranging from 2.39406 to 2.4058 PHz. This variation emphasizes the potential of PHz imaging in effectively distinguishing between

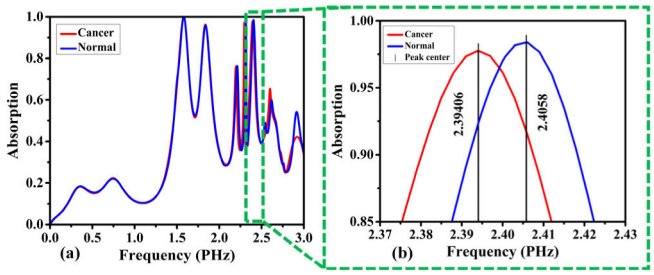


Fig. 23. Detection of absorption coefficients by the proposed biosensor for normal blood and blood cancer within the frequency range of (a) 0–3 PHz and (b) 2.37–2.43 PHz.

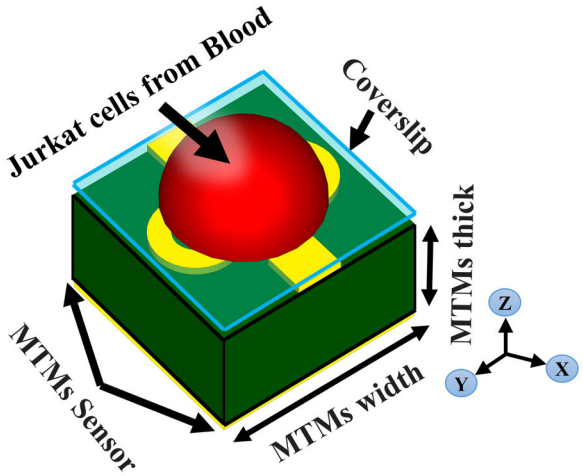


Fig. 24. Utilization of the MWI approach for diagnosing blood cancer.

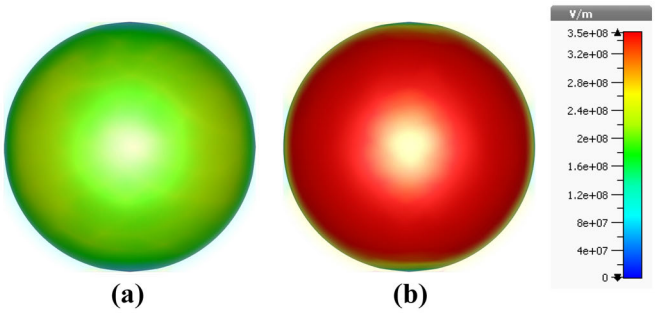


Fig. 25. *E*-field results of the MWI technique. (a) Normal blood and (b) blood cancer.

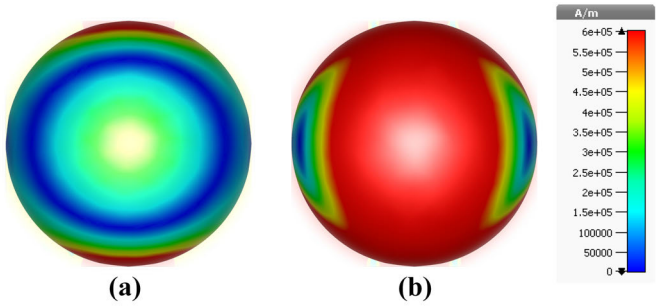


Fig. 26. *H*-field results of the MWI technique. (a) Normal blood and (b) blood cancer.

healthy and cancerous tissues, offering valuable insights for diagnostic and therapeutic interventions.

The proposed triple-band PHz biosensor exhibits high absorption efficiency with minimal dependence on the incident angle of EM radiation. This angular insensitivity, achieved through MTM structure optimization and resonator design, ensures robust and consistent detection performance across varying orientations. While the sensor's field distribution is optimized for uniform absorption, sample positioning and orientation relative to the sensor can influence detection sensitivity. Localized field interactions may introduce signal variations if the sample is misaligned with high-field regions, potentially impacting the detection of small anomalies. To mitigate these effects, future implementations may incorporate positioning calibration mechanisms, such as controlled sample holders, to ensure optimal and reproducible sample placement. Subsequent studies will parametrically simulate the impact of sample misalignment, including lateral displacements and angular tilts, on diagnostic accuracy. This investigation of spatial sensitivity will inform the development of enhanced positioning strategies for experimental validation, ultimately strengthening the biosensor's translational potential for early-stage leukemia detection.

The proposed biosensor differentiates leukemia-affected from healthy blood samples based on resonance frequency shifts rather than absolute absorption values. While absorption characteristics provide insight into sensor performance, their variability due to sample preparation and experimental conditions can introduce uncertainties, leading to inconsistencies in diagnostic accuracy. The reliance on operator expertise further compounds these challenges.

To address these limitations, the biosensor exploits the intrinsic dielectric properties of biological samples, which remain constant regardless of preparation methods. Structural and compositional differences in leukemia cells alter their dielectric properties, inducing measurable shifts in resonance frequencies. Full-wave EM simulations reveal significant frequency shifts at 1.605, 1.848, and 2.424 PHz when exposed to malignant samples.

These shifts provide a robust and reproducible diagnostic metric, offering a reliable framework for early-stage leukemia detection. By emphasizing resonance-based analysis, this study enhances the sensor's specificity and stability, ensuring accurate differentiation between malignant and healthy cells.

The study's findings were validated using MWI methods that reconstruct images within the PHz frequency range. This approach allows for detailed visualization. In this setup, Jurkat cells from the blood are placed on the PHz MTM absorber (Fig. 24). When PHz radiation is applied, the distribution of electric and magnetic fields varies depending on the presence of cancer, as shown in Figs. 25 and 26, for different resonance frequencies. The color-coded representation indicates the intensity of the electric and magnetic fields, with blue indicating low intensity and red indicating high intensity. The images reveal that the electric field intensity is higher in the presence of cancer cells, as seen in Fig. 25(b), where the color red is prominent. This suggests that cancer cells absorb more radiation than normal cells. The difference in

dielectric properties between leukemia cells and normal blood cells is due to variations in cell membrane composition, cytoplasmic content, cell morphology, and cellular activity. Leukemia cells exhibit altered lipid and protein composition, affecting membrane capacitance and conductivity. Differences in ion permeability, higher metabolic activity, and variations in intracellular ionic concentrations and macromolecules also contribute. Morphological characteristics and resting membrane potential further influence the dielectric response. The rapid division of leukemia cells contrasts with the stable state of normal blood cells, resulting in distinct dielectric properties, useful for diagnostic and monitoring techniques in hematological disorders. These characteristics result in greater absorption of PHz radiation by cancerous tissue compared to normal tissue. Therefore, the resonance mode at different PHz is sensitive to the presence of cancerous cells in the blood, which can be detected through magnetic field imaging. The imaging techniques clearly demonstrate that the densities of electric and magnetic fields vary based on the presence of cancer cells. In comparison to normal blood cells, the electric and magnetic fields are less concentrated. Thus, when cells are affected by cancer, they tend to absorb more PHz radiation, and the intensity of these fields can be effectively utilized to diagnose the presence of cancer.

The proposed sensor presents its results in the form of images that highlight different properties. In particular, Fig. 25 showcases the electric field data obtained through MWI. In Fig. 25(a), the electric field of normal blood is depicted as weak. However, Fig. 25(b) displays a bright red spot, indicating a significantly higher electric field density, which suggests the presence of leukemia. This demonstrates that MWI can effectively differentiate between healthy blood tissue and cancerous tissue by measuring the electric field. The ability to identify and distinguish malignant tissues is crucial for the early detection and effective treatment of leukemia. Moreover, this capability allows for noninvasive real-time monitoring of tissue abnormalities, which is especially valuable in the early diagnosis and detection of leukemia. Additionally, MWI has clinical applications beyond diagnosis, as it can also be utilized to evaluate treatment response.

Further inquiries were carried out to validate the results. An in-depth analysis of the magnetic field is depicted in Fig. 26. In Fig. 26(a), a low-intensity magnetic field area suggests the existence of healthy blood. On the other hand, Fig. 26(b) shows a filled red area, indicating a high level of magnetic field, which implies leukemia. Subsequent investigations on the connection between magnetic field intensity and leukemia have revealed a significant link between high magnetic field areas and the disease. These findings suggest that magnetic field analysis can serve as a diagnostic tool for leukemia.

To systematically refine the biosensor's structural parameters and achieve optimal performance, an iterative optimization framework was implemented. The process is illustrated in Fig. 27, which outlines the key steps involved in parameter selection, full-wave EM simulations, performance evaluation, and convergence verification. The optimization algorithm ensures that the biosensor attains high sensitivity, triple-band operation, and near-perfect absorption at the designated PHz frequencies. By continuously adjusting geometric and material parameters based on resonance shifts and absorption characteristics, the algorithm fine-tunes the design for maximal diagnostic accuracy. This structured approach enables precise control over the biosensor's response to leukemia-affected and healthy samples, ensuring reliable differentiation. The inclusion of Fig. 27 provides a clear visualization of this process, enhancing the interpretability of the optimization methodology employed in this study.

TABLE II
BIOSENSING PERFORMANCE COMPARISONS OF VARIOUS SENSOR APPLICATIONS BASED ON MTM

| Ref. | Year Published | FOM (RIU−1) | Q | S (THz/RIU) | Bio-application |
|---|---|---|---|---|---|
| [79] | 2014 | 0.1216 | 5.58 | 0.02432 | detection of Penicillia |
| [80] | 2020 | - | - | 0. 960 | Biosensor, Collagen |
| [81] | 2020 | 1.88 | 6.6 | 0.285 | sensor |
| [20] | 2021 | - | 10.64 | 1.65 | Cancer detection |
| [82] | 2021 | - | - | 0. 2833 | Polystyrene particle |
| [83] | 2022 | 0.166 | - | 1.06 | detection of avian influenza virus |
| [84] | 2022 | - | - | 0.068 | Hepatocellular carcinoma |
| [85] | 2022 | 1.81, 1.57 | 8.21, 6.05 | 0. 203 | sensor |
| [21] | 2022 | 3.86 | 13 | 0.207 | Cancer detection |
| [19] | 2022 | 2.75 | 2.43 | 1.21 | Cancer Diagnosi, Biosensor |
| [86] | 2023 | - | 11 | 0.278 | Bovin serum albumin protein |
| [18] | 2023 | - | 82 | 0.495 | Cancer detection |
| [32] | 2023 | 0.86, 1.15 | 12.8, 13.5 | 0.0515, 0.076 | Non-Melanoma Skin Cancer Diagnostics |
| [35] | 2024 | 1.186, 4.656 | 7.81, 12.84 | 138, 440.5 | Non-Melanoma Skin Cancer Diagnostics |
| [49] | 2025 | 6.3, 3 | 85.77, 41.46 | 0.049, 0.068 | Cervical cancer |
| This work | - | 1.11<br>58.265<br>7.518 | 7.61<br>72.93<br>21.73 | 234.285<br>1476.428<br>838.571 | Blood cancer Diagnostics |

## VIII. FUTURE PERSPECTIVE

The development of biosensors with enhanced sensitivity is crucial for the early detection of various cancers, such as early-stage adrenal gland cancer (PC-12), colon cancer, breast cancer, cervical cancer (HeLa), and nonmelanoma skin cancer. Utilizing PHz EM wave imaging techniques, these advanced biosensors aim to improve diagnostic accuracy and timeliness.

## IX. BENCHMARKING

The field of biosensors for early cancer detection is advancing rapidly, with a focus on enhancing sensitivity and specificity. A notable innovation is the proposed nano-biosensor operating in the PHz band with triple-band functionality, each band achieving over 98% absorbance. This triple-band configuration improves detection accuracy by differentiating biomolecular signatures, reducing false positives and negatives. Each band independently enhances detection, ensuring subtle cancerous changes are identified precisely.

Performance metrics such as sensitivity, quality factor ($Q$-factor), and figure of merit (FOM) show substantial improvements compared to previous THz range sensors, as

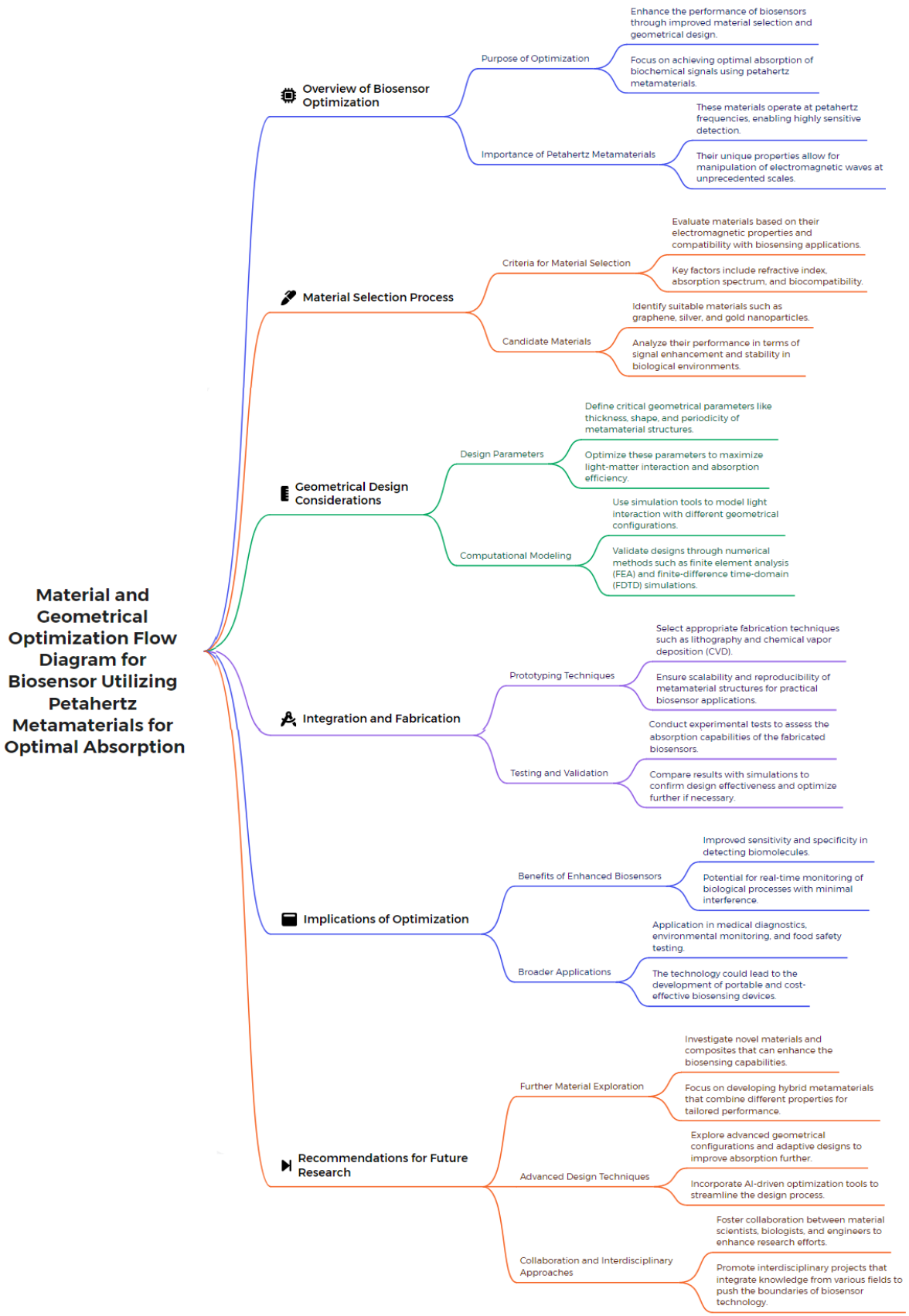


Fig. 27. Optimization framework for biosensor design and performance enhancement.

illustrated in Table II. The higher energy and shorter wavelengths of PHz waves facilitate stronger biomolecule interactions and superior spatial resolution, crucial for early-stage cancer detection. Unique spectral fingerprints in the PHz range, not observable in the THz regime, further enhance specificity.

Integrating MTMPA technology with $SiO_2$ substrates and silver-based resonators, this biosensor is highly sensitive and significantly miniaturized, promising advancements in clinical diagnostics. This MTM-based nano-biosensor could revolutionize early cancer detection, offering superior performance and miniaturization for earlier and more accurate leukemia and cancer detection.

## X. Conclusion

The main goal of this research was to develop an innovative, miniaturized biosensor for MWI applications. Specifically, we targeted early-stage detection of leukemia. The proposed sensor was designed with the limitations of the existing devices in mind, such as the limited spatial resolution of imaging. The device features a dipole and two rings made of gold or silver mounted on a $SiO_2$ dielectric substrate with a fully metallic backplane. This article elaborates on the evolution of the biosensor's topology and comprehensive simulation studies conducted using a commercial full-wave EM solver. The operating principles are elucidated through parametric studies, analyses of absorption and refraction characteristics, discussions of electric and magnetic fields, and surface current density distributions.

The key properties of the proposed design that make it stand out from the solutions available in the literature include

1) The operation in the PHz range.
2) Triple-band functionality with resonant frequencies around 1.61, 1.85, and 2.42 PHz.
3) Achieving near-perfect absorption rates at the resonant frequencies.
4) Insensitivity to the angle of incidence.

It was possible to achieve this functionality and performance by carefully selecting the sensor's materials and architecture and meticulously optimizing its geometry parameters. Furthermore, comprehensive full-wave simulations of the MWI system incorporating our device demonstrate its suitability for blood cancer diagnostics, highlighting the sensor's ability to distinguish between healthy and cancerous samples through noticeable frequency shifts in absorption responses. Finally, extensive benchmarking against state-of-the-art biosensors, as reported in recent literature, has been carried out. It does corroborate that the proposed device significantly improves spectral properties and achieves remarkable spatial resolution due to its PHz range operation, outperforming the benchmark sensors.

## Acknowledgment

Musa N. Hamza is with the Department of Physics, College of Science, University of Raparin, Sulaymaniyah 46012, Iraq (e-mail: musa.nuraden@uor.edu.krd).

Mohammad Tariqul Islam is with the Department of Electrical, Electronic and Systems Engineering, Faculty of Engineering and Built Environment, Universiti Kebangsaan Malaysia (UKM), Bangi, Selangor 43600, Malaysia (e-mail: tariqul@ukm.edu.my).

Sunil Lavadiya is with the Department of Information and Communication Technology, Marwadi University, Rajkot, Gujarat 360003, India (e-mail: sunil.lavadiya@marwadieducation.edu.in).

Iftikhar ud Din is with the Department of Telecommunication Engineering, University of Engineering and Technology, Mardan 23200, Pakistan (e-mail: iftikharuddin114@gmail.com).

Bruno Cavalcante de Souza Sanches is with the Department of Electronic Systems Engineering, Escola Politécnica da Universidade de São Paulo, São Paulo 05508-010, Brazil (e-mail: bruno.csanches@usp.br).

Slawomir Koziel is with the Engineering Optimization and Modeling Center, Reykjavik University, 102 Reykjavik, Iceland, and also with the Faculty of Electronics, Telecommunications and Informatics, Gdansk University of Technology, 80-233 Gdansk, Poland (e-mail: Koziel@ru.is).

Syeda Iffat Naqvi is with the Department of Telecommunication Engineering, University of Engineering and Technology, Taxila 47050, Pakistan (e-mail: iffat.naqvi@uettaxila.edu.pk).

Ali Farmani is with the Department of Electronics Engineering, Lorestan University, Khorramabad 68151-44316, Iran (e-mail: farmani.a@lu.ac.ir).

Md. Shabiul Islam is with the Faculty of Engineering (FOE), Multimedia University (MMU), Cyberjaya, Selangor 63100, Malaysia (e-mail: shabiul.islam@mmu.edu.my).

## References

[1] M. J. Thun, J. O. DeLancey, M. M. Center, A. Jemal, and E. M. Ward, "The global burden of cancer: Priorities for prevention," *Carcinogenesis*, vol. 31, no. 1, pp. 100–110, Jan. 2010.

[2] F. Bray, J. Ferlay, I. Soerjomataram, R. L. Siegel, L. A. Torre, and A. Jemal, "Global cancer statistics 2018: GLOBOCAN estimates of incidence and mortality worldwide for 36 cancers in 185 countries," *CA Cancer J. Clinicians*, vol. 68, no. 6, pp. 394–424, 2018.

[3] H. Zhao, D. Wang, W. Du, D. Gu, and R. Yang, "MicroRNA and leukemia: Tiny molecule, great function," *Crit. Rev. Oncol./Hematol.*, vol. 74, no. 3, pp. 149–155, Jun. 2010.

[4] J. J. Hutter, "Childhood leukemia," *Pediatrics Rev.*, vol. 31, no. 6, pp. 234–241, 2010.

[5] C. Dieter, E. D. Lourenco, and N. E. Lemos, "Association of long non-coding RNA and leukemia: A systematic review," *Gene*, vol. 735, Apr. 2020, Art. no. 144405.

[6] Y. Zhao, Y. Wang, and S. Ma, "Racial differences in four leukemia subtypes: Comprehensive descriptive epidemiology," *Sci. Rep.*, vol. 8, no. 1, p. 548, Jan. 2018.

[7] J. Okikiolu, R. Dillon, and K. Raj, "Acute leukaemia," *Medicine*, vol. 49, no. 5, pp. 274–281, 2021.

[8] F. Huang, P. Guang, F. Li, X. Liu, W. Zhang, and W. Huang, "AML, ALL, and CML classification and diagnosis based on bone marrow cell morphology combined with convolutional neural network: A STARD compliant diagnosis research," *Medicine*, vol. 99, no. 45, Nov. 2020, Art. no. e23154.

[9] E. Jabbour, S. O'Brien, M. Konopleva, and H. Kantarjian, "New insights into the pathophysiology and therapy of adult acute lymphoblastic leukemia," *Cancer*, vol. 121, no. 15, pp. 2517–2528, Aug. 2015.

[10] I. Abunadi and E. M. Senan, "Multi-method diagnosis of blood microscopic sample for early detection of acute lymphoblastic leukemia based on deep learning and hybrid techniques," *Sensors*, vol. 22, no. 4, p. 1629, Feb. 2022.

[11] B. Ghafari, M. Danaie, and M. Afsahi, "Perfect absorber based on epsilon-near-zero metamaterial as a refractive index sensor," *Sens. Imag.*, vol. 24, no. 1, p. 15, May 2023.

[12] Z. Vafapour et al., "The potential of refractive index nanobiosensing using a multi-band optically tuned perfect light metamaterial absorber," *IEEE Sensors J.*, vol. 21, no. 12, pp. 13786–13793, Jun. 2021.

[13] M. Berka et al., "A miniaturized folded square split ring resonator cell based dual band polarization insensitive metamaterial absorber for C- and Ku-band applications," *Opt. Quantum Electron.*, vol. 55, no. 8, p. 699, Aug. 2023.

[14] Z. Vafapour, E. S. Lari, and M. R. Forouzeshfard, "Breast cancer detection capability of a tunable perfect semiconductor absorber: Analytical and numerical evaluation," *Opt. Eng.*, vol. 60, no. 10, Oct. 2021, Art. no. 107101.

[15] M. Li, H.-L. Yang, X.-W. Hou, Y. Tian, and D.-Y. Hou, "Perfect metamaterial absorber with dual bands," *Prog. Electromagn. Res.*, vol. 108, pp. 37–49, 2010.

[16] L. Xie, W. Gao, J. Shu, Y. Ying, and J. Kono, "Extraordinary sensitivity enhancement by metasurfaces in terahertz detection of antibiotics," *Sci. Rep.*, vol. 5, no. 1, p. 8671, Mar. 2015.

[17] S. J. Park, S. H. Cha, G. A. Shin, and Y. H. Ahn, "Sensing viruses using terahertz nano-gap metamaterials," *Biomed. Opt. Exp.*, vol. 8, no. 8, pp. 3551–3558, 2017.

[18] Z. Mezache, Z. Hafdi, and J. Tao, "Design of a novel graphene buzzle metamaterial refractometer for sensing of cancerous cells in the terahertz regime," *Optik*, vol. 287, Sep. 2023, Art. no. 171170.

[19] C. Tan et al., "Cancer diagnosis using terahertz-graphene-metasurface-based biosensor with dual-resonance response," *Nanomaterials*, vol. 12, no. 21, p. 3889, Nov. 2022.

[20] M. Y. Azab, M. F. O. Hameed, A. M. Nasr, and S. S. A. Obayya, "Highly sensitive metamaterial biosensor for cancer early detection," *IEEE Sensors J.*, vol. 21, no. 6, pp. 7748–7755, Mar. 2021.

[21] S. K. Patel, J. Surve, and J. Parmar, "Detection of cancer with graphene metasurface-based highly efficient sensors," *Diamond Rel. Mater.*, vol. 129, Nov. 2022, Art. no. 109367.

[22] M. N. Hamza et al., "Designing a high-sensitivity microscale triple-band biosensor based on terahertz MTMs to provide a perfect absorber for non-melanoma skin cancer diagnostic," *IEEE Photon. J.*, vol. 16, no. 2, pp. 1–13, Apr. 2024.

[23] B. Amini and Z. Atlasbaf, "Design and analysis of high-sensitivity tunable graphene sensors for cancer detection," *Opt. Quantum Electron.*, vol. 55, no. 5, p. 446, May 2023.

[24] M. N. Hamza and M. T. Islam, "Design of MTM-based multiband micro-biosensor in terahertz region as perfect absorber for early-stage leukemia diagnosis with sensitivity 18626373 THz/RIU," *IEEE Sensors J.*, vol. 24, no. 10, pp. 16055–16069, May 2024.

[25] P. Upender and A. Kumar, "THz dielectric metamaterial sensor with high Q for biosensing applications," *IEEE Sensors J.*, vol. 23, no. 6, pp. 5737–5744, Mar. 2023.

[26] M. N. Hamza, S. Koziel, and A. Pietrenko-Dabrowska, "Design and experimental validation of a metamaterial-based sensor for microwave imaging in breast, lung, and brain cancer detection," *Sci. Rep.*, vol. 14, no. 1, p. 16177, Jul. 2024.

[27] Z. Geng, X. Zhang, Z. Fan, X. Lv, and H. Chen, "A route to terahertz metamaterial biosensor integrated with microfluidics for liver cancer biomarker testing in early stage," *Sci. Rep.*, vol. 7, p. 16378, Nov. 2017.

[28] S. Banerjee, U. Nath, P. Dutta, A. V. Jha, B. Appasani, and N. Bizon, "A theoretical terahertz metamaterial absorber structure with a high quality factor using two circular ring resonators for biomedical sensing," *Inventions*, vol. 6, no. 4, p. 78, Nov. 2021.

[29] H. Emami Nejad, A. Mir, and A. Farmani, "Supersensitive and tunable nano-biosensor for cancer detection," *IEEE Sensors J.*, vol. 19, no. 13, pp. 4874–4881, Jul. 2019.

[30] D. Li et al., "Identification of early-stage cervical cancer tissue using metamaterial terahertz biosensor with two resonant absorption frequencies," *IEEE J. Sel. Topics Quantum Electron.*, vol. 27, no. 4, pp. 1–7, Jul. 2021.

[31] S. Banerjee, P. Dutta, A. V. Jha, B. Appasani, and M. S. Khan, "A biomedical sensor for detection of cancer cells based on terahertz metamaterial absorber," *IEEE Sensors Lett.*, vol. 6, no. 6, pp. 1–4, Jun. 2022.

[32] M. N. Hamza and M. T. Islam, "Designing an extremely tiny dual-band biosensor based on MTMs in the terahertz region as a perfect absorber for non-melanoma skin cancer diagnostics," *IEEE Access*, vol. 11, pp. 136770–136781, 2023.

[33] A. Chaudhuri, B. Rai, and P. Pal, "Design of a dual-band metasurface cross-polarization converter for cancer detection in the terahertz band," *IEEE Sensors J.*, vol. 24, no. 6, pp. 7292–7298, Jun. 2023.

[34] J. Chen, F. Hu, X. Ma, M. Yang, S. Lin, and A. Su, "Deep neural network-assisted terahertz metasurface sensors for the detection of lung cancer biomarkers," *IEEE Sensors J.*, vol. 24, no. 10, pp. 15698–15705, May 2024.

[35] M. N. Hamza, M. T. Islam, S. Lavadiya, S. Koziel, I. U. Din, and B. C. de Souza Sanches, "Designing a high-sensitivity dual-band nano-biosensor based on petahertz MTMs to provide a perfect absorber for early-stage nonmelanoma skin cancer diagnostic," *IEEE Sensors J.*, vol. 24, no. 11, pp. 18418–18427, Jun. 2024.

[36] A. Hlali, A. Oueslati, and H. Zairi, "Numerical simulation of tunable terahertz graphene-based sensor for breast tumor detection," *IEEE Sensors J.*, vol. 21, no. 8, pp. 9844–9851, Apr. 2021.

[37] X. Hou et al., "Cancer biomarkers ultrasensitive detection based on terahertz frequency-comb-like," *IEEE Sensors J.*, vol. 23, no. 10, pp. 10413–10419, May 2023.

[38] M. N. Hamza et al., "Development of a terahertz metamaterial micro-biosensor for ultrasensitive multispectral detection of early stage cervical cancer," *IEEE Sensors J.*, vol. 24, no. 20, pp. 32065–32079, Oct. 2024.

[39] A. Veeraselvam, G. N. A. Mohammed, K. Savarimuthu, and P. D. Vijayaraman, "An ultra-thin multiband refractive index-based carcinoma sensor using THz radiation," *IEEE Sensors J.*, vol. 22, no. 3, pp. 2045–2052, Feb. 2022.

[40] M. N. Hamza et al., "Ultra-compact quintuple-band terahertz metamaterial biosensor for enhanced blood cancer diagnostics," *PLoS ONE*, vol. 20, no. 1, Jan. 2025, Art. no. e0313874.

[41] D. Xie et al., "Terahertz metamaterial biosensor with double resonant frequencies for specific detection of early-stage hepatocellular carcinoma," *IEEE Sensors J.*, vol. 23, no. 2, pp. 1124–1131, Jan. 2023.

[42] F. Wahaia et al., "Detection of colon cancer by terahertz techniques," *J. Mol. Struct.*, vol. 1006, nos. 1–3, pp. 77–82, Dec. 2011.

[43] M. N. Hamza et al., "Terahertz dual-band metamaterial biosensor for cervical-cancer diagnostics," *IEEE Photon. J.*, vol. 16, no. 5, pp. 1–11, Oct. 2024.

[44] M. Rezeg, A. Hlali, and H. Zairi, "THz biomedical sensing for early cancer detection: Metamaterial graphene biosensors with rotated split-ring resonators," *IEEE Photon. J.*, vol. 16, no. 4, pp. 1–10, Aug. 2024.

[45] L. Yu et al., "The medical application of terahertz technology in non-invasive detection of cells and tissues: Opportunities and challenges," *RSC Adv.*, vol. 9, no. 17, pp. 9354–9363, 2019.

[46] G. Valušis, A. Lisauskas, H. Yuan, W. Knap, and H. G. Roskos, "Roadmap of terahertz imaging 2021," *Sensors*, vol. 21, no. 12, p. 4092, Jun. 2021.

[47] W. Zhang et al., "Terahertz metamaterials for biosensing applications: A review," *Biosensors*, vol. 14, no. 1, p. 3, Dec. 2023.

[48] M. N. Hamza, M. T. Islam, and S. Koziel, "Advanced sensor for non-invasive breast cancer and brain cancer diagnosis using antenna array with metamaterial-based AMC," *Eng. Sci. Technol., Int. J.*, vol. 56, Aug. 2024, Art. no. 101779.

[49] M. N. Hamza et al., "Design and validation of ultra-compact metamaterial-based biosensor for non-invasive cervical cancer diagnosis in terahertz regime," *PLoS ONE*, vol. 20, no. 2, Feb. 2025, Art. no. e0311431.

[50] S. T. Foroughi, R. Yadipour, S. Golmohammadi, and T. Nurmohammadi, "Slow light realization based on plasmon-induced transparency in Γ-shaped rectangular resonator structures," *Plasmonics*, vol. 19, no. 2, pp. 785–791, Apr. 2024.

[51] Z. Vafapour and A. Zakery, "New regime of plasmonically induced transparency," *Plasmonics*, vol. 10, no. 6, pp. 1809–1815, Dec. 2015.

[52] Z. Zhu and X. Yi, "All-optical multichannel switch and slow light based on dynamically tunable plasmon-induced transparency," *Appl. Opt.*, vol. 63, no. 19, pp. 5029–5038, 2024.

[53] Z. Vafapour and A. Zakery, "New approach of plasmonically induced reflectance in a planar metamaterial for plasmonic sensing applications," *Plasmonics*, vol. 11, no. 2, pp. 609–618, Apr. 2016.

[54] Y. Huang, S. Zhong, T. Shi, Y.-C. Shen, and D. Cui, "Terahertz plasmonic phase-jump manipulator for liquid sensing," *Nanophotonics*, vol. 9, no. 9, pp. 3011–3021, Jul. 2020.

[55] Z. Vafapour, "Cost-effective bull's eye aperture-style multi-band metamaterial absorber at sub-THz band: Design, numerical analysis, and physical interpretation," *Sensors*, vol. 22, no. 8, p. 2892, Apr. 2022.

[56] Q. Wang, Y. Chen, J. Mao, F. Yang, and N. Wang, "Metasurface-assisted terahertz sensing," *Sensors*, vol. 23, no. 13, p. 5902, Jun. 2023.

[57] Z. Xu, Y. Wang, S. Liu, J. Ma, S. Fang, and H. Wu, "Metamaterials with analogous electromagnetically induced transparency and related sensor designs—A review," *IEEE Sensors J.*, vol. 23, no. 7, pp. 6378–6396, Apr. 2023.

[58] A. Rahman, M. T. Islam, M. J. Singh, S. Kibria, and M. Akhtaruzzaman, "Electromagnetic performances analysis of an ultra-wideband and flexible material antenna in microwave breast imaging: To implement a wearable medical bra," *Sci. Rep.*, vol. 6, no. 1, p. 38906, Dec. 2016.

[59] Z. Vafapour, W. Troy, and A. Rashidi, "Colon cancer detection by designing and analytical evaluation of a water-based THz metamaterial perfect absorber," *IEEE Sensors J.*, vol. 21, no. 17, pp. 19307–19313, Sep. 2021.

[60] S. Nourinovin, M. M. Rahman, M. Naftaly, M. P. Philpott, Q. H. Abbasi, and A. Alomainy, "Highly sensitive terahertz metasurface based on electromagnetically induced transparency-like resonance in detection of skin cancer cells," *IEEE Trans. Biomed. Eng.*, vol. 71, no. 7, pp. 2180–2188, Jul. 2024.

[61] N. Rajaram, J. S. Reichenberg, M. R. Migden, T. H. Nguyen, and J. W. Tunnell, "Pilot clinical study for quantitative spectral diagnosis of non-melanoma skin cancer," *Lasers Surg. Med.*, vol. 42, no. 10, pp. 876–887, 2010.

[62] I. V. A. K. Reddy, S. Elmaadawy, E. P. Furlani, and J. M. Jornet, "Photothermal effects of terahertz-band and optical electromagnetic radiation on human tissues," *Sci. Rep.*, vol. 13, no. 1, p. 14643, Sep. 2023.

[63] M. Gezimati and G. Singh, "Advances in terahertz technology for cancer detection applications," *Opt. Quantum Electron.*, vol. 55, no. 2, p. 151, Feb. 2023.

[64] R. Contractor, G. D'Aguanno, and C. Menyuk, "Ultra-broadband, polarization-independent, wide-angle absorption in impedance-matched metamaterials with anti-reflective moth-eye surfaces," *Opt. Exp.*, vol. 26, no. 18, pp. 24031–24043, 2018.

[65] R. M. H. Bilal, M. A. Saeed, M. A. Naveed, M. Zubair, M. Q. Mehmood, and Y. Massoud, "Nickel-based high-bandwidth nanostructured metamaterial absorber for visible and infrared spectrum," *Nanomaterials*, vol. 12, no. 19, p. 3356, Sep. 2022.

[66] I. Tathfif, M. F. Hassan, K. S. Rashid, A. A. Yaseer, and R. H. Sagor, "A highly sensitive plasmonic refractive index sensor based on concentric triple ring resonator for cancer biomarker and chemical concentration detection," *Opt. Commun.*, vol. 519, Sep. 2022, Art. no. 128429.

[67] M. M. K. Shuvo et al., "Polarization and angular insensitive bendable metamaterial absorber for UV to NIR range," *Sci. Rep.*, vol. 12, no. 1, p. 4857, Mar. 2022.

[68] H. Liu, K. Luo, S. Tang, D. Peng, F. Hu, and L. Tu, "An ultra-wideband THz/IR metamaterial absorber based on doped silicon," *Materials*, vol. 11, no. 12, p. 2590, Dec. 2018.

[69] A. Musa et al., "Broadband plasmonic metamaterial optical absorber for the visible to near-infrared region," *Nanomaterials*, vol. 13, no. 4, p. 626, Feb. 2023.

[70] S. Patel, S. K. Patel, A. H. M. Almawgani, A. Armghan, A. Alzahrani, and S. A. Taya, "Numerical study of graphene-based wideband solar absorber using MIM structure for solar thermal energy conversion," *Adv. Theory Simul.*, vol. 7, no. 1, Jan. 2024, Art. no. 2300352.

[71] M. S. Raeen, A. Nella, and R. Maheswar, "A fourfold star petal–shaped polarization-insensitive broadband plasmonic metamaterial absorber," *Plasmonics*, vol. 18, no. 3, pp. 1059–1074, Jun. 2023.

[72] I. H. Chowdhury, M. M. R. Mazumder, S. S. Islam, M. T. Islam, M. S. Soliman, and M. S. Islam, "Ultrawideband nanostructured metamaterial absorber with an octagon-packed star-shaped resonator for UV to NIR spectrum wavelength application," *Ain Shams Eng. J.*, vol. 15, no. 4, Apr. 2024, Art. no. 102653.

[73] M. Danaie and B. Kiani, "Design of a label-free photonic crystal refractive index sensor for biomedical applications," *Photon. Nanostruct.-Fundam. Appl.*, vol. 31, pp. 89–98, Sep. 2018.

[74] K. Ahmed, B. K. Paul, F. Ahmed, M. A. Jabin, and M. S. Uddin, "Numerical demonstration of triangular shaped photonic crystal fibre-based biosensor in the terahertz range," *IET Optoelectron.*, vol. 15, no. 1, pp. 1–7, Feb. 2021.

[75] M. A. Jabin et al., "Surface plasmon resonance based titanium coated biosensor for cancer cell detection," *IEEE Photon. J.*, vol. 11, no. 4, pp. 1–10, Aug. 2019.

[76] P. Kumar, V. Kumar, and J. S. Roy, "Dodecagonal photonic crystal fibers with negative dispersion and low confinement loss," *Optik*, vol. 144, pp. 363–369, Sep. 2017.

[77] T. Parvin, K. Ahmed, A. M. Alatwi, and A. N. Z. Rashed, "Differential optical absorption spectroscopy-based refractive index sensor for cancer cell detection," *Opt. Rev.*, vol. 28, no. 1, pp. 134–143, Feb. 2021.

[78] P. Sharma, P. Sharan, and P. Deshmukh, "A photonic crystal sensor for analysis and detection of cancer cells," in *Proc. Int. Conf. Pervasive Comput. (ICPC)*, Jan. 2015, pp. 1–5.

[79] S. J. Park et al., "Detection of microorganisms using terahertz metamaterials," *Sci. Rep.*, vol. 4, no. 1, p. 4988, May 2014.

[80] S. Asgari, N. Granpayeh, and T. Fabritius, "Controllable terahertz cross-shaped three-dimensional graphene intrinsically chiral metastructure and its biosensing application," *Opt. Commun.*, vol. 474, Nov. 2020, Art. no. 126080.

[81] T. Chen, D. Zhang, F. Huang, Z. Li, and F. Hu, "Design of a terahertz metamaterial sensor based on split ring resonator nested square ring resonator," *Mater. Res. Exp.*, vol. 7, no. 9, Sep. 2020, Art. no. 095802.

[82] J. Yang and Y.-S. Lin, "Design of tunable terahertz metamaterial sensor with single- and dual-resonance characteristic," *Nanomaterials*, vol. 11, no. 9, p. 2212, Aug. 2021.

[83] E. Hoseini, A. Mir, and A. Farmani, "Modeling and proposal of a black phosphorus-based nanostructure for detection of avian influenza virus in infrared region," *Opt. Quantum Electron.*, vol. 54, no. 10, p. 609, Oct. 2022.

[84] R. Bhati and A. K. Malik, "Ultra-efficient terahertz metamaterial sensor," *Results Opt.*, vol. 8, Aug. 2022, Art. no. 100236.

[85] H. Hu, B. Qi, Y. Zhao, X. Zhang, Y. Wang, and X. Huang, "A graphene-based THz metasurface sensor with air-spaced structure," *Frontiers Phys.*, vol. 10, Sep. 2022, Art. no. 990126.

[86] Y. Shen et al., "Low-concentration biological sample detection using an asymmetric split resonator terahertz metamaterial," *Photonics*, vol. 10, no. 2, p. 111, Jan. 2023.

**Musa N. Hamza** received the B.Sc. degree from the Department of Physics, Faculty of Science and Health, Koya University, Koysinjaq, Erbil, Iraqi Kurdistan, Iraq, in 2015, and the M.Sc. degree from the Department of Medical Physics, College of Medical and Applied Sciences, Charmo University, Chamchamal, Sulaymaniyah, Iraq, in 2023.

His research interests include medical physics, the diagnosis of different types of cancer at an early stage, antenna arrays, metamaterials, sensors, and biosensors.

**Mohammad Tariqul Islam** (Senior Member, IEEE) is currently a Professor with the Department of Electrical, Electronic and Systems Engineering, Universiti Kebangsaan Malaysia (UKM), Bangi, Malaysia, and a Visiting Professor with the Kyushu Institute of Technology, Fukuoka, Japan. He has authored and co-authored about 600 research journal articles, nearly 250 conference papers, and few book chapters on various topics related to antennas, metamaterials, and microwave imaging with 25 inventory patents filed. Thus far, his publications have been cited 15 700× and have an H-index of 56 (Source: Scopus). His Google scholar citation is 25 000 and H-index is 66. He was a recipient of more than 40 research grants from the Malaysian Ministry of Science, Technology and Innovation, Ministry of Education, UKM research grant, international research grants from Japan, Saudi Arabia, and Kuwait. He has supervised about 50 Ph.D. theses, 30 M.Sc. theses, and has mentored more than ten postdoctoral and visiting scholars. He has developed the Antenna Measurement Laboratory that includes antenna design and measurement facility till 40 GHz. His research interests include communication antenna design, metamaterial, satellite antennas, and microwave imaging.

Dr. Islam served as an Executive Committee Member for IEEE AP/MTT/EMC Malaysia Chapter, from 2019 to 2020, the Chartered Professional Engineer (CEng), a fellow of IET, U.K., and a Senior Member of IEICE, Japan. He received several International Gold Medal Awards, a Best Invention in Telecommunication Award for his research and innovation, and best researcher awards at UKM. He was a recipient of 2018, 2019, and 2020 IEEE AP/MTT/EMC Malaysia Chapter, Excellent Award. He also won the Best Innovation Award and the Best Researcher Award by UKM, in different years. He was a recipient of Publication Award from Malaysian Space Agency, in several years. He was an Associate Editor of *IET Electronics Letter*. He serves as a Guest Editor for *Sensors Journal* and *Nanomaterials*, and an Associate Editor for IEEE ACCESS.

**Sunil Lavadiya** (Member, IEEE) received the B.Tech. degree in electronics and communication from Saurashtra University, Rajkot, India, in 2008, the M.Tech. degree in communication engineering from Nirma University, Rajkot, in 2010, and the Ph.D. degree in electronics and communication engineering from Marwadi University, Rajkot, Gujarat, in 2022, on the topic of High Gain Frequency Reconfigurable Liquid Metamaterial Microstrip Patch Antenna.

He is working as an Associate Professor with the Department of Information and Communication Technology, Marwadi University. He has adapted to all aspects of Electronics and Communication Engineering, including training, education, and research. He works in the MIMO, sensors, reconfigurable, superstrate, solar absorber, and liquid antennas. He has published 50 SCI research articles, 12 SCOPUS index articles, eight book chapters, and five papers in an international conference and filed four design patents and one copyright.

Dr. Lavadiya is a member of IETE.

**Iftikhar ud Din** received the B.Sc. and M.Sc. degrees in telecommunication engineering from the University of Engineering and Technology, Peshawar, Pakistan, in 2017 and 2021, respectively.

He is a member of the Antennas and Microwave Engineering Research Group (AMERG) in UET Mardan. His current research interests include UWB antennas, FSS-based UWB antennas and sub-6-GHz 5G antennas, 5G millimeter wave antennas and MIMO antennas, frequency selective surfaces, EBGs, and metamaterial-based antenna.

**Bruno Cavalcante de Souza Sanches** (Member, IEEE) received the B.S. degree in information engineering and the M.Sc. degree in energy from the Federal University of ABC, Santo André, Brazil, in 2011 and 2013, respectively, and the Ph.D. degree in microelectronics from the Integrated Systems Laboratory (LSI), University of São Paulo, São Paulo, Brazil, in 2021, working in the design of a novel mixed signal integrated circuit used in the ALICE experiment in the CERN LHC.

He has more than 15 years of experience in electronics and microelectronics design. He has been involved in hardware development, smart grids, algorithms, artificial intelligence, digital communication systems, EDA tools, electronics for high energy physics experiments, and in several systems targeting early cancer detection including bioimpedance spectroscopy and microwave imaging.

**Slawomir Koziel** (Fellow, IEEE) received the M.Sc. and Ph.D. degrees in electronic engineering from Gdansk University of Technology, Gdansk, Poland, in 1995 and 2000, respectively, and the M.Sc. degree in theoretical physics and mathematics and the Ph.D. degree in mathematics from the University of Gdansk, Gdansk, in 2002 and 2003, respectively.

He is currently a Professor with the Department of Engineering, Reykjavik University, Reykjavik, Iceland. His research interests include CAD and modeling of microwave and antenna structures, simulation-driven design, surrogate-based optimization, space mapping, circuit theory, analog signal processing, evolutionary computation, and numerical analysis.

**Syeda Iffat Naqvi** (Senior Member, IEEE) received the Ph.D. degree in telecommunication engineering from the University of Engineering and Technology, Taxila, Pakistan, in 2021.

She is currently serving as an Assistant Professor at the University of Engineering and Technology, Taxila. She is working toward the design and implementation of MIMO antennas systems for millimeter-wave 5G and beyond wireless communication applications, metamaterials, terahertz and subterahertz antennas, beamsteerable antenna arrays, and ridge gap waveguide-based antennas. She has authored and co-authored numerous technical articles in ISI-indexed journals, and delivered a number of conference talks. She is also a frequent reviewer of various prestigious journals. Furthermore, she has served as a technical committee member for a number of international conferences and a guest editor for various special journal issues.

**Ali Farmani** (Member, IEEE) received the B.Sc. degree in electrical engineering from the Shiraz University of Technology, Shiraz, Iran, in 2008, the M.Sc. degree in electrical engineering from the University of Tabriz, Tabriz, Iran, in 2010, and the Ph.D. degree in electrical engineering from Shiraz University, Shiraz, in 2017.

He was an Assistant Professor at Lorestan University, Khorramabad, Iran, from 2018 to 2024, and he has mentored several B.Sc. theses, ten M.Sc. theses, and four Ph.D. dissertations. He has authored or co-authored more than 106 ISI papers and three book chapters. His research interests are VLSI, nanoelectronics, plasmonics, and investigation of new materials for integrated photonics.

Dr. Farmani was a recipient of the Fellowship for Ph.D. Study at Shiraz University, as an Exceptional Talent. He was also a recipient of the Excellent Reviewer Award from Elsevier and IEEE Journals from 2017 to 2024. He received the Shiraz Distinguished Ph.D. Dissertation Award for his work on plasmonic nanostructures.

**Md. Shabiul Islam** (Senior Member, IEEE) received the B.Sc. (Hons.) and M.Sc. degrees from the Department of Applied Physics and Electronics, Rajshahi University, Bangladesh, in 1985 and 1986, respectively, the M.Sc. degree (by research) in microcontroller-based system design from the Department of Electrical, Electronics and System Engineering, Universiti Kebangsaan Malaysia (UKM), Bangi, Malaysia, in 1997, and the Ph.D. degree in VLSI design from the Faculty of Engineering (FOE), Multimedia University (MMU), Cyberjaya, Malaysia, in 2008.

From 1991 to 1993, he was a Scientific Officer with the Institute of Electronics and Material Science (IEMS), Bangladesh Atomic Energy Commission (BAEC), Saver, Dhaka, Bangladesh. From July 1999 to July 2009, he was a Lecturer with the Faculty of Engineering, MMU. From July 2009 to March 2012, he was a Senior Lecturer with IMEN, UKM. From June 2010 to December 2012, he was an Associate Fellow with the Department of Electrical, Electronics and System Engineering, Faculty of Engineering and Built Environment, UKM. From March 2012 to December 2016, he worked as an Associate Professor with the Institute of Microengineering and Nanoelectronics (IMEN), UKM, where he was an Associate Fellow, from April 2017 to March 2020. He is currently a Professor with the FOE, MMU. He is also the Head of the Micro/Nano Electronics System (MiNES) Laboratory, IMEN. His expertise covers a wide range of engineering disciplines, including micro/nanosystem design, VLSI design, microcontroller-based system design, micro-powering harvesting, and digital communication system. He received internal and external research funds for doing his research work at IMEN, UKM, from 2010 to 2016. His research support also partly contributed to the award of the Higher Education Center of Excellence (HiCOE) from the Malaysian government to IMEN recently. He has published 78 ISI and SCOPUS, five research books, one chapter in book, and 90 conference proceeding. He filed one patent.

Dr. Islam is a member of the IEEE Circuits and Systems Society and Bangladesh Electronics Society, and an Associate Member of Bangladesh Computer Society (AM476).